Marine Pollution Bulletin 222 (2026) 118574

Contents lists available at ScienceDirect

Marine Pollution Bulletin

journal homepage: www.elsevier.com/locate/marpolbul

Dispersion monitoring services in the Mediterranean Sea: A multi-model statistical approach

Beatrice Maddalena Scotto [a,b,*], Andrea Lira Loarca [b], Antonio Novellino [a], Giovanni Besio [b]

[a] ETT S.p.A., Via Enrico Albereto 21, Genoa, 16153, Italy
[b] DICCA, University of Genoa, Via Montallegro 1, Genoa, 16145, Italy

ARTICLE INFO

Keywords:
Oil spill
Ocean dynamics
Stokes drift
OceanParcels

ABSTRACT

The Mediterranean Sea is increasingly impacted by shipborne pollution, necessitating sophisticated oil spill monitoring systems. This study presents a detailed framework for assessing oil spill dynamics in the Mediterranean using various oceanographic models. The first part compares oil dispersion results using sea surface current data from Copernicus Marine Environment Monitoring Service (CMEMS), Naval Hydrographic and Oceanographic Service (SHOM), and French Research Institute for the Exploitation of the Sea (IFREMER). The second part evaluates particle dispersion simulations, improving upon previous results by incorporating Stokes drift and wind drag effects from the Copernicus ERA5 and the MeteOcean model, operational at DICCA Unige. The study also calculates the centroid of each oil slick to track its trajectory over time and assessing its spatial and temporal deformation. To validate the methodology, a practical case study is conducted, comparing the results with Sentinel-1 satellite images from the first days after the accident and with press reports. The results demonstrate that both Stokes drift and wind significantly influence the surface transport of oil spill, improving trajectory predictions when combined with surface currents. In addition, comparison between ocean and climate models revealed substantial variability in dispersion results, highlighting the importance of model selection in operational forecasting or the benefits of the use of a multi-model probabilistic approach.

1. Introduction

The Mediterranean Sea serves as a vital hub for maritime transits and recorded a significant increase in maritime transport in recent years: according to the most recent data, vessel traffic has increased by an average of 3.0–3.5% per year, peaking at around 4.0% in 2019 (Deandreis et al., 2022). Although transit experienced a significant decline in 2020 due to the pandemic, it fully recovered by 2021: the Mediterranean Sea accounts for approximately 10% of global cruises, which carried around 2.5 million passengers in 2019 and 19% of the world's freight traffic, mainly along the North African coast (Wecel et al., 2024). Mediterranean ports handle over 1.3 billion tonnes of goods annually, including 697 million tonnes of liquid bulk, which accounts for 40% of short sea shipping in 2022 (EUROSTAT, 2024). Major ports, such as the Port of Valencia, handled over 12.2 million tonnes of goods in the first two months of 2024 alone, highlighting the increasing cargo volumes across the region (Valenciaport, 2024). Tanker traffic plays a crucial role in this, with approximately 7.5 million barrels of oil per day (10% of global seaborne oil) transiting the Suez Canal in 2023 (IEA, 2023). Italy and Spain each handle more than 137 million tonnes of liquid bulk annually, further underscoring the significance of tanker traffic in Mediterranean trade routes (EUROSTAT, 2024). The high volume of maritime traffic in the Mediterranean Sea exerts considerable pressure on an already fragile ecosystem. As shipping activity increases, so do environmental concerns, including acoustic and chemical pollution, an increased risk of collisions with marine life, and oil spills that can severely impact marine biodiversity.

A recent report from the European Maritime Safety Agency (EMSA) recorded approximately 2,066 oil spills of varying magnitudes in the Mediterranean between 2015 and 2017, highlighting the persistent threat of marine pollution in the region (Polinov et al., 2021). However, even a single spill can cause severe environmental damage. The extent of damage caused by an oil spill depends on several factors: the quantity of oil spilled, its behavior in the marine environment, the chemicals involved, the sensitivity of the affected marine area, and the wind and weather conditions at the time of the incident. Improving precision and quality of oil dispersion fate prediction is crucial for limiting the environmental impact of accidental spills. Central to this research is the dispersal of oil spills in marine areas and the modulating role of

* Corresponding author at: DICCA, University of Genoa, Via Montallegro 1, Genoa, 16145, Italy.
E-mail address: beatrice.scotto@edu.unige.it (B.M. Scotto).

https://doi.org/10.1016/j.marpolbul.2025.118574
Received 17 February 2025; Received in revised form 1 August 2025; Accepted 8 August 2025
Available online 24 September 2025

sea surface currents, wind, and wave action. It is important to note that wave action involves both the horizontal transport of buoyant oil (i.e. Stokes drift) and the vertical intrusion into the water column (Cao et al., 2021). In this study, the former is considered by including Stokes drift in the Lagrangian simulations. The exclusion of vertical mixing processes reflects a deliberate simplification of the oil transport mechanism, aimed at focusing on surface dynamics within a two-dimensional framework.

A review of oil spill tracking methods highlights the significance of Lagrangian particle models, which are widely used to simulate the transport and dispersion of oil in marine environments. These models track the fate of oil particles under the influence of ocean currents, wind, and turbulence, providing detailed insights into oil spill dynamics GNOME (General NOAA Operational Modelling Environment), a widely used model, simulates the fate and transport of spilled oil by integrating both environmental and chemical processes (Beegle-Krause, 2001). MEDSLIK-II, another well-known Lagrangian model used in the Mediterranean Sea, predicts oil spill trajectories and assesses risks by incorporating hydrodynamic and atmospheric data (De Dominicis et al., 2013). The OILTRANS model focuses on simulating the transport and degradation of oil spills in 3D hydrodynamic environments (Berry et al., 2012). OpenDrift, a more recent framework, enables the simulation of oil and other substances' trajectories in complex oceanic environments using advanced Lagrangian tracking techniques. (Dagestad et al., 2018).

Nevertheless, few studies have systematically compared the impact of different input datasets—such as atmospheric forcing, ocean currents, and wind fields—on the performance of these models. One study, using MEDSLIK-II, investigated the impact of different ocean and atmospheric forcings on oil spill simulations, showing significant variability in the results depending on the quality and resolution of the input data (Lyubartseva et al., 2015). Some studies have shown improved accuracy in oil spill simulations when wind, Stokes drift and sea surface currents are combined. Abascal et al. (2009) showed that the inclusion of these forcings significantly improved model predictions when calibrated against drift data during the Prestige oil spill. Similarly, Yang et al. (2021) highlighted the critical role of Stokes drift in improving trajectory predictions during the Sanchi oil spill. These results emphasize the importance of integrating multiple environmental forcings to enhance oil spill trajectory modeling. Increasing the accuracy of ocean prediction models is fundamental to improving oil spill response strategies and mitigating environmental impacts. These tools are pillars of the Blue Economy, offering potential for economic growth, environmental sustainability, job creation, and active support in decision-making (Novellino et al., 2024).

The primary objective of this study is to compare various oceanographic forcing datasets by applying a consistent methodology to evaluate their efficiency and accuracy in predicting the temporal evolution of oil spills—an essential component for effective marine pollution prevention and preparedness. This study employs a Lagrangian Particle Tracking (LPT) model (Van Sebille et al., 2023), recognized for its effectiveness in replicating real-world scenarios, to extrapolate the probabilistic distribution of oil spill trajectories. The results focus on the 2018 Capo Corso collision, which caused significant environmental damage by releasing approximately 600 cubic meters of heavy fuel oil into the Mediterranean Sea, impacting marine ecosystems and coastal areas (REMPEC, 2019). Key metrics such as the centroid of spill clusters and their spatial distribution, are analyzed. This paper is structured as follows: Section 2 presents the different oceanographic and atmospheric datasets used as input for the LPT model; Section 3 describes the analysis using the Particle Tracking Model (PTM) and the methodology used to evaluate the characteristics and evolution of the spill; Section 4 describes the real-case scenario used to validate the methodology and Section 5 presents the results. Finally, Section 6 presents the conclusions and the discussion of this study.

2. Data

The complexity of modeling the ocean dynamics leads to considerable variability in the results depending on the models employed to describe the different physical processes. Different current fields obtained through different oceanographic models are then adopted. The main sources of inaccuracy include (i) the non-linearity of the Navier–Stokes equations and the chaotic nature of the ocean circulation, that can lead to large temporal and spatial differences due to small variations in initial conditions (Visconti and Ruggieri, 2020), (ii) the lack of small-scale resolution that leads to a parametrization of turbulent dynamics and no information at the sub-grid scale (Furuichi and Hibiya, 2015), (iii) the uncertainties in forcing fields, initial conditions, and boundary conditions can introduce errors in the representation of ocean state variables, particularly in regional models that depend on larger-scale simulations for their boundary conditions (Moore et al., 2011). To overcome these drawbacks, ocean models adopt various strategies, including stochastic approaches where undefined parameters are determined by a probability distribution, and data assimilation techniques that minimize errors by comparing with real ocean data using methods such as HF radar or drifter (Sayol et al., 2014; Berta et al., 2014).

2.1. Currents

This study utilizes three distinct datasets from different ocean circulation models to compare their effectiveness in reproducing oil spill trajectories. These datasets are selected based on their spatial resolution, temporal coverage, and availability of essential variables. The analysis evaluates how well each model represents ocean currents that influence spill dispersion. All model data used in this study are freely available, ensuring accessibility and facilitating broader application. Specifically, sea surface current data from the following models are used:

- Copernicus Marine Environment Monitoring Service (CMEMS)
- Naval Hydrographic and Oceanographic Service (SHOM)
- French Research Institute for the Exploitation of the Sea (IFREMER)

The sea surface current dataset used from the Copernicus Marine Service (CMEMS) is the Mediterranean Sea Physics Reanalysis (Med MFC). The horizontal grid resolution of the model is 1/24° (about 4–5 km) and the unevenly spaced vertical levels are 141 (Escudier et al., 2020). For the present study only the surface level is used. The temporal resolution of the model is one hour. This model is forced with the ECMWF ERA5 climate model and data assimilation includes observations from satellite altimetry, in situ temperature, and salinity profiles.

The second dataset, provided by SHOM (SHOM) (Shom, 2017), is based on the HYCOM 3D (Hybrid Coordinate Ocean Model). This model, referred to as HYDRODYN-SURF_HYCOM3D-SURF_R2000_MEDOC-NOR, is a specific configuration of HYCOM designed to simulate sea surface velocity with an hourly temporal resolution. It provides daily forecasts and operates at a spatial resolution of approximately 1.8 km. While the model does not generate reanalysis data, its archived outputs – available from January 1, 2016 – represent the best analyses obtained from weekly simulations, with data assimilation applied only after June 2022. The model is forced by the atmospheric data from ECMWF, specifically utilizing the ERA5 reanalysis for wind fields, surface pressure, and other meteorological variables. Additionally, data assimilation is incorporated from satellite observations, including sea surface height (SSH) derived from altimetry, sea surface temperature (SST), and in situ temperature and salinity profiles.

The third dataset, provided by IFREMER (IFREMER) (Garnier et al., 2014), was developed as part of the MARC project, Modelling and Analysis for Coastal Research. This dataset is based on the Ifremer MARS3D

model, which simulates ocean circulation, biogeochemistry, and sediment dynamics, along with the WAVEWATCH III wave model. The latter was developed by an international consortium coordinated by NOAA, with contributions from the LOPS (Laboratory for Ocean Physics and Satellite Remote Sensing) research unit. The ocean circulation model has a spatial resolution of approximately 1.2 km and a temporal resolution of three hours. The MARS3D model is forced by atmospheric data from the ECMWF ERA5 reanalysis, which provides wind fields, surface pressure, and other meteorological parameters essential for surface forcing. Additionally, it is coupled with the WAVEWATCH III model to account for wave effects, particularly in coastal regions. The model also integrates data assimilation from various sources, including satellite-derived sea surface temperature, sea surface height from altimetry, and in situ temperature and salinity profiles from the European Marine Observation and Data network — Physics (Míguez et al., 2019).

2.2. Wind and waves

For the wave-induced Stokes drift and the 10m-wind, two models with very different spatial resolution have been used: the first ERA5 is the fifth generation ECMWF reanalysis for the global climate and weather for the past eight decades, produced by the European Centre for Medium-Range Weather Forecasts (ECMWF) and distributed in the Copernicus Climate Change Service (C3S) (Hersbach et al., 2020). An estimate of uncertainty is provided by a 10-member ensemble, where each member runs the model with slight variations in observational data and parameters, producing a set of simulations every three hours to account for uncertainty related to observational and model errors. The spatial resolution of the atmospheric data is 31 km (0.28125°) for the high-resolution forecast (HRES), while the ensemble of data assimilation (EDA) has a resolution of 63 km (0.5625°). For wave data, ERA5 uses a different grid, with a resolution of 0.36 degrees for HRES and 1.0 degree for EDA. The two variables used are the 10-m wind velocity ($\vec{u}_w$) and the Stokes drift ($\vec{u}_s$).

The second model is the atmospheric and wave hindcast developed by the MeteOcean research group of the University of Genoa (Italy). The atmospheric modeling and downscaling is done with the non-hydrostatic mesoscale Weather Research and Forecast (WRF) model version 3.4 (Skamarock et al., 2008) with an approximately 10-km resolution Lambert Conic Conformal grid over the entire Mediterranean Sea. Initial and boundary conditions are obtained from the National Center for Environmental Prediction (NCEP) Climate Forecast System Reanalysis for the period 01/01/1979 – 31/03/2011 (Saha et al., 2010, CFSR) and Climate Forecast System Version 2 01/04/2011 – 31/12/2020 (Saha et al., 2014, CFSv2) with a 3–hour and $0.5 \times 0.5°$ temporal and spatial resolution, respectively. For additional details of the WRF model configuration and its performance in the Mediterranean Sea the reader is referred to Cassola et al. (2016), Ferrari et al. (2020). The wind fields from the WRF model are used as forcing for the third-generation wave model Wavewatch III (version 5.16; Tolman et al., 2014, hereinafter WW3) with the source terms of growth/dissipation ST4 (Ardhuin et al., 2010; Rascle and Ardhuin, 2013) providing hourly wave climate integrated parameters, i.e. significant wave height H_s, from 1979 to 2024 in the Mediterranean Sea using a regular grid of longitude 0.127° and latitude 0.09°, corresponding to ≈ 10 km (Mentaschi et al., 2013, 2015; Besio et al., 2016; Lira-Loarca et al., 2022).

3. Methods

3.1. Particle tracking model

The particle dispersion simulation is analyzed using the Lagrangian Particle Tracking Model Ocean Parcels, which effectively simulates the displacement of virtual particles influenced by ocean currents. This model utilizes Eulerian fluid information, such as velocity fields, to integrate particles' trajectories (Van Sebille et al., 2018). Various interpolation techniques, including bilinear, trilinear, and spline interpolation, are employed to create continuous velocity fields within grid cells. To accurately estimate the dispersion velocity of an oil slick, it is essential to consider not only the surface current component but also the wind at 10 meters above the surface and the Stokes drift. This is because these factors significantly influence the movement of the oil slick. To account for these processes, the east and north components of the velocity field are calculated as follows,

$$\vec{u} = \vec{u}_c + \alpha \cdot \vec{u}_s + \beta \cdot \vec{u}_w, \tag{1}$$

where $\vec{u}_c$ is the sea surface current velocity, $\vec{u}_s$ is the Stokes velocity, $\vec{u}_w$ is the wind velocity, while α and β are respectively the Stokes and wind coefficients.

The MeteOcean-UniGe hindcast does not contain the Stokes drift data, so the latter is calculated through the variables in the dataset. Since the case study is mainly in a deep water region, Eq. (2) for the Stokes drift approximation is applied (Kumar et al., 2017)

$$[U_s, V_s] = \sigma \cdot ka^2 \cdot \exp(2kz) \cdot [\cos(\theta), \sin(\theta)], \tag{2}$$

where σ is the dispersion number, in deep water evaluated as $\sigma^2 = g \cdot k$, k is the wavenumber, g is the gravitational acceleration, $a = H_s/2$ is the wave amplitude, z is the water depth and θ is the peak wave direction.

The Eq. (1) allows for the quantification of the relative contributions of each factor to the overall movement of the oil slick, providing a more comprehensive understanding of the complex interactions at play. By incorporating these additional contributions, the accuracy of our predictions can be improved, ultimately informing more effective decision-making in oil spill response and environmental damage assessment. The movement of particles is influenced by advection and diffusion. Advection refers to the horizontal transport of particles driven by ocean and wind currents, which primarily determines the trajectory of the particles. Diffusion describes the spread of particles due to their individual irregular movements. Dispersion, representing the overall trend of particle clusters, increases rapidly over short to intermediate time scales and linearly over larger scales, eventually reaching a constant value (Abernathey et al., 2022; Lacasce and Mahadevan, 2006). In this study, the diffusion coefficient are selected based on the model's resolution and considered as small-scale noise affecting particle movements.

The PTM is implemented through OceanParcels, a tool designed to simulate the trajectories of passive particles. The key components of the model used in this study include the representation of particle motion within an existing flow field based on hydrodynamic data. Specifically, eastward (u) and northward (v) surface velocities are used to simulate horizontal particle motion. Horizontal diffusivity is parameterized by the Kh_zonal and $Kh\_meridional$ fields, representing zonal and meridional diffusivity, respectively. The $AdvectionDiffusionEM$ kernel, based on the Euler–Maruyama scheme, is used in this study to integrate the particle motion, including both advection and diffusion processes. The equation governing the diffusion component of particle movement is the following:

$$\Delta x_{diff} = \sqrt{2, K_h \cdot \Delta t} \cdot \mathcal{N}(0, 1) \tag{3}$$

where Δx_{diff} is the stochastic displacement due to sub-grid scale diffusion, K_h is the local horizontal diffusivity, a combination of Kh_zonal and $Kh\_meridional$ from the input data, Δt is the time step and $\mathcal{N}(0, 1)$ is a random value drawn from a standard normal distribution, introducing the stochastic noise. This approach adds a random walk component to the particles, simulating the sub-grid scale diffusion due to small-scale turbulence that cannot be resolved directly by the model's grid. In addition, the process of subdiffusion, characterized by the sublinear growth of the mean square displacement (Hulianytskyi, 2022), is included in the diffusivity term and accounted for within the OceanParcels kernel. To accurately approximate the diffusivity gradient, the parameter $dres$ is used to compute the central difference of the diffusivity field and

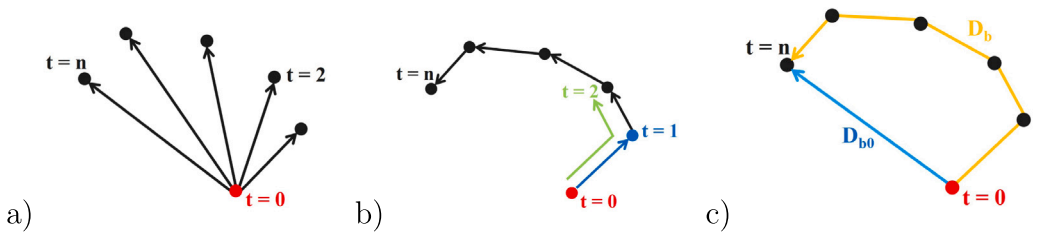

Fig. 1. (a)Absolute distance; (b) Relative distance; (c) Comparison between absolute and relative distance at the final time step.

depends on the model grid size. The value of *dres* is chosen to be significantly smaller than the spatial resolution of the data to ensure accurate representation of the diffusivity gradient. (Van Sebille et al., 2023). To simplify the analysis, virtual particles without mass are considered. The first step in the analysis is to design a system capable of representing the probability distribution of particles in selected areas. The probability distribution is achieved by constructing a regular grid within the analysis region. Finally, the simulation runs over a defined period of time with a specific time step to simulate real conditions observed in the field.

3.2. Mixing processes

The aim of the following analysis is to provide detailed information on the characteristics and movement of an oil slick.

Once the particles trajectories are obtained through OceanParcels, the probability density map is constructed. For each time step, the number of particles passing through each grid cell (areal bin) is counted and normalized by dividing by the total number of particles present in the entire domain area. This method evaluates the probability density, calculated by Eq. (4), resulting in an experimental distribution that reflects the dispersion patterns of the particles:

$$P(x, y, t) = \frac{n(x, y, t)}{N} \tag{4}$$

where n is the number of particles present in a single cell, corresponding to a single simulation, and is both space and time dependent. N is the total number of particles released at the beginning of the simulation. This is employed to construct a map of the distinct probability of each model simulation and to determine which area exhibits a higher concentration of particles.

The centroid of each individual cloud of dispersed particles is then calculated as the average of the x an y positions of the particles present in the cloud, at each time step. Specifically, the components of the centroid, $\bar{x}(t)$, $\bar{y}(t)$, are evaluated using Eqs. (5) as follows

$$\bar{x}(t) =< x_i(t) >, \quad \bar{y}(t) =< y_i(t) > \tag{5}$$

where $x_i(t)$ and $y_i(t)$ are the coordinates of the i-nth particle at the time t. From the centroids information the absolute and relative distances can be computed, in order to evaluate the trajectory covered by the simulations. The absolute distance (D_{b0}) represents the displacement of each centroid from its initial position over time (Fig. 1 a). The relative distance, D_b, is defined as the sum of the individual segments connecting each centroid to the next one.

Consequently, the absolute distance, D_{b0}, is defined following Eq. (6)

$$D_{\mathrm{b0}}(t) = \sqrt{(\bar{x}(t) - \bar{x}(0))^2 + (\bar{y}(t) - \bar{y}(0))^2} \tag{6}$$

where $(\bar{x}(t), \bar{y}(t))$ is the position of centroid over time and $(\bar{x}(0), \bar{y}(0))$ is the position of centroid at time zero. The relative distance instead provides the measure of the total path traveled by the centroid up to time t and is represented by Eq. (7)

$$D_{\mathrm{b}}(t) = \sum_{j=1}^{t} \sqrt{(\bar{x}(j) - \bar{x}(j-1))^2 + (\bar{y}(j) - \bar{y}(j-1))^2} \tag{7}$$

where $\bar{x}(j)$ and $\bar{y}(j)$ are the coordinates of the centroid at time j.

Another mixing property of interest in this study is the overall displacement of the particles, i.e. the degree of dispersion. Specifically, the relative dispersion of the particles with respect to the position of the centroid over time is calculated (Eq. (8)).

$$R^2(t) = R_x^2(t) + R_y^2(t) \tag{8}$$

The two components of Eq. (8) are the dispersion in time in the direction of x and in the direction of y, respectively, and are reported in Eq. (9)

$$R_x^2(t) =< (x_i(t) - \bar{x}(t))^2 >, \quad R_y^2(t) =< (y_i(t) - \bar{y}(t))^2 > \tag{9}$$

where $x_i(t)$ and $y_i(t)$ represent the position of the i-nth particle at time t. $\bar{x}(t)$ and $\bar{y}(t)$ correspond to the position of the centroid of the cluster at each single time t. The relative dispersion will allow to measure quantitatively the spread of the particle cloud, capturing both the magnitude of the dispersion and the directions in which the particles are spreading. It helps to assess the anisotropy of the deformation of the cluster along its trajectory, indicating whether the dispersion is more along certain directions or uniform.

As satellite images are available, an accuracy analysis of the simulations is also conducted by comparing the output obtained with the data recorded by the SAR sensors. To achieve this, the distance in kilometers is evaluated between the centroids of particle dispersion simulations and the centroid of the observed SAR image for the temporal instants available (Eq. (10)).

$$D_{\mathrm{centroid}} = \sqrt{(\bar{x}(t) - x_{\mathrm{SAR}})^2 + (\bar{y}(t) - y_{\mathrm{SAR}})^2} \tag{10}$$

where $(\bar{x}(t), \bar{y}(t))$ are the coordinates of the simulation centroid at the given instant and $(x_{\mathrm{SAR}}, y_{\mathrm{SAR}})$ are the coordinates of the SAR image centroid. This provide a quantitative measure of spatial agreement between simulated and observed oil spill locations. The number of simulated particles intersecting the slick detected by Sentinel-1 is also calculated for each of the three time instants.

The ratio N_{in} N_{tot}, representing the proportion of particles within the SAR slick, is also determined.

$$P_{\mathrm{in}} = \frac{N_{\mathrm{in}}}{N_{\mathrm{tot}}} \times 100 \tag{11}$$

where P_{in} represents the percentage of particles, N_{in} is the number of particles inside the SAR image, and N_{tot} is the total number of particles for the specific simulation. This value is expressed as a percentage (Eq. (11)), and indicates the ability of the simulations to reproduce the observed spill.

4. Case study

A real-case scenario is analyzed to validate the proposed methodology. The selected case study is the collision that occurred on October 7, 2018, at 07:00 UTC between two vessels off the coast of Corsica in the Northern Tyrrhenian Sea (Mediterranean Sea), as shown in Fig. 2.

At the time of the collision, the weather conditions were optimal with perfect visibility (10-m wind speed under 2 m/s). The collision occurred in French waters, 30 km north-east of Cap Corse. The two

Fig. 2. Left panel: Geographic location of the collision site (43° 14′94" N, 9° 28′47" E). Top right panel: Depiction of the ship collision at the moment of impact (REMPEC, 2019). Bottom right panel: Evidence of hydrocarbon contamination observed on the shore of Pampelonne Beach, France, following the collision (CEDRE, 2019).

vessels involved were the ro-ro ferry Ulysses, owned by a Tunisian company, and the container vessel CLS Virginia, owned by Cyprus Sea Lines, which was at anchor. The impact caused a spill of six hundred tonnes of fuel from the hull over a distance of about 20 kilometers. Despite the monitoring and clean-up operations carried out by the Coast Guard, the oil slick was carried by the currents for many kilometers in the Ligurian Sea, westwards towards the French coast. A few days later, on the morning of the 16th of October, hydrocarbons from the accident were detected on the beach at Pampelonne, near Saint-Tropez (CEDRE, 2019). The area affected by the incident is part of an area with an extremely fragile ecosystem of great environmental interest, specifically the Pelagos Sanctuary, which is recognized for its significant biodiversity and the presence of various marine mammals (Fossi et al., 2013). For validation and calibration, the following reliable sources are used: satellite imagery from Sentinel-1 SAR sensors captured during the first three days after the incident, and multiple reports of hydrocarbon beaching along the French coastline. The first confirmed observation was recorded on October 16 at Pampelonne Beach near Saint-Tropez, with subsequent detections reported in surrounding areas in the following days.

5. Results

The study explores two distinct scenarios of forcing conditions. The first scenario is driven solely by sea surface currents ($\vec{u}_c$), offering insights into the horizontal motion of the ocean for all three ocean circulation models described in Section 2.1. The second scenario takes a more comprehensive approach, incorporating all relevant forcings: sea surface currents ($\vec{u}_c$), wind fields at 10-meter height ($\vec{u}_w$), and Stokes drift ($\vec{u}_s$). Wind and wave data are obtained from the MeteOcean-UniGe and ERA5 datasets, as detailed in Section 2.2. This resulted in six different simulations, combining the three current models (CMEMS, SHOM, and IFREMER) with the two wind-wave models (ERA5 and MeteOcean-UniGe).

The analysis is simplified by modeling an instantaneous dispersion, rather than a gradual and continuous release as would occur in a real event, since no information is available regarding the temporal evolution of the release itself. All simulations are carried out using the same consistent framework and configuration. Each model run began at the same time on 7 October 2018 at 07:00 UTC, from the same release location at 43° 14′94"N, 9° 28′47"E, with 800 particles released instantly and a simulation duration of 13 days.

5.1. Oil spill dispersion forced by surface currents alone

Fig. 3 shows the temporal evolution of the oil spill and the probability density map (Eq. (4)) for the simulations forced with the three ocean circulation models used in the analysis: the CMEMS (blue), SHOM (green) and IFREMER (red). At the initial stages, the concentration is at its highest due to the instantaneous release from the source. However, the values remain relatively low because the particles are initially distributed over a large area, spanning more than one grid cell, as estimated using the first available satellite images. Over time, this concentration decreases significantly as the particles disperse over a larger area. The significance of this study lies in identifying the areas with the highest pollutant concentration, which in Fig. 3 reach values of ~ 0.008. This information can help to guide the implementation of containment measures in response to such emergencies. A significant difference in the temporal evolution of the oil slick can be observed between simulations corresponding to the three current forcings (IFREMER, SHOM, and CMEMS), as shown in Fig. 3. This variation is primarily due to the inherent challenges in modeling highly variable ocean currents and the subgrid-scale estimates. Even small variations in the initial conditions can lead to substantially different outcomes. Despite these differences, all models generally show a westward movement towards the French coast. This behavior is primarily driven by the dominant mesoscale circulation patterns in the Mediterranean Sea during the simulation period. These mesoscale structures, such as persistent eddies and large-scale current systems, operate at spatial and temporal scales that govern the overall transport of surface waters (Millot and Taupier-Letage, 2005). While the detailed trajectories differ due to model-specific dynamics and resolution, the main advection pathway remains similar, leading the simulated oil spills towards the same general impact area. Notably, the IFREMER simulation reached greater distances more quickly than both the CMEMS

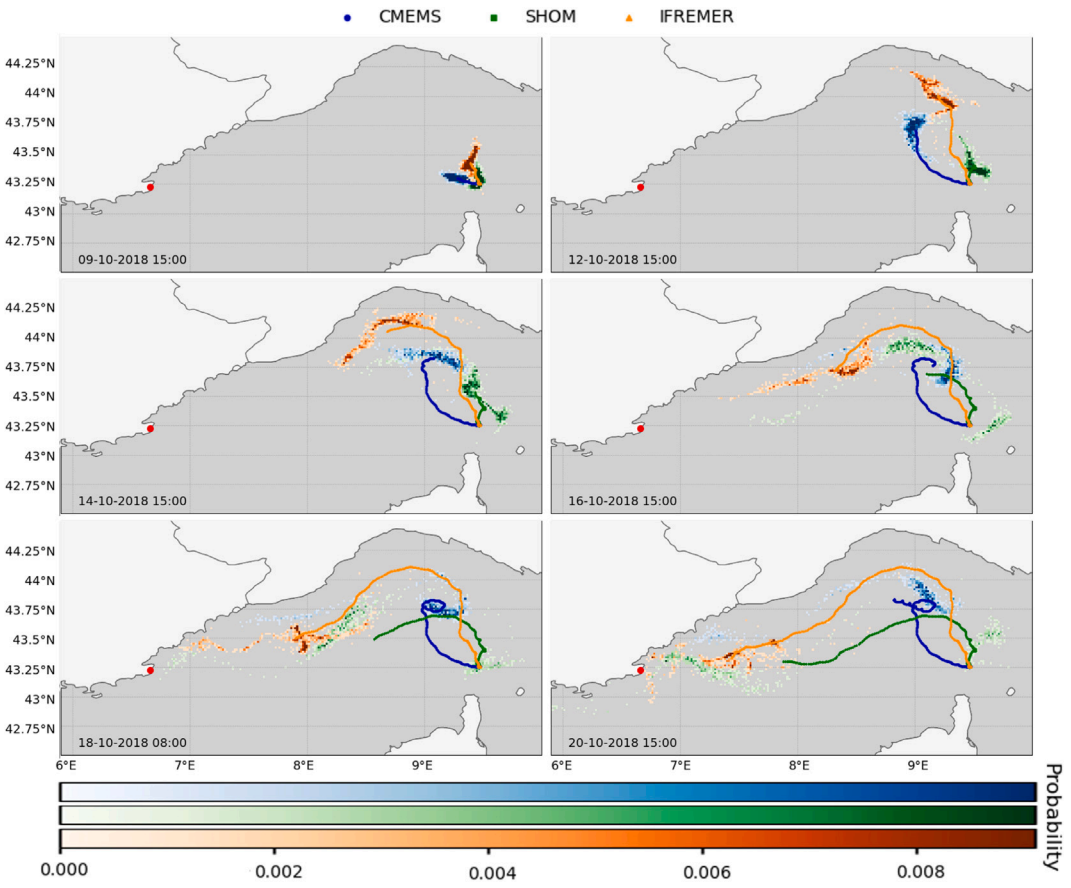

Fig. 3. Evolution of oil spills with relative probability for the three models and trajectory followed by the centroid, considering only sea surface currents forcing. From top-left to bottom-right: 09/10/2018 15:00, 12/10/2018 15:00, 14/10/2018 15:00, 18/10/2018 15:00, 20/10/2018 08:00, 23/10/2018 08:00. The red dot represents the area of impact on the beach of Pampelonne in France, when traces were found on the 16/10/2018 presumably in the early morning. (For interpretation of the references to color in this figure legend, the reader is referred to the web version of this article.)

and SHOM simulations. The duration of the event is based on actual observations, as crude oil was found on the beach at Pampelonne (marked by the red dot on the map) on October 16, more than a week after the incident. However, none of the three simulations predicted the oil slick reaching the coastline by that date, suggesting that additional forcing factors, not accounted for in this currents-only scenario, may have influenced the spill's trajectory. After a two-day delay, on the 18 October, both the IFREMER at 23:00, and SHOM at 01:00 simulations depicted particles near the French coast, likely impacting the Saint-Tropez promontory. The CMEMS model showed a larger delay compared to the other two, as the oil spill is directed into a vortex between Corsica and Liguria, arriving on the near the coast on the 22 October at 23:00. Although the SHOM model uses archived forecast data instead of reanalysis products, its results are not significantly different from those of the CMEMS and IFREMER models. In fact, the SHOM simulations predict the impact area around the same time as IFREMER, suggesting that SHOM performs reliably as a forecasting tool, even when compared to reanalysis-based models. It is important to note that even though the CMEMS and IFREMER models are based on reanalysis data, they exhibit noticeable differences in trajectories and dispersion patterns. This highlights the inherent variability between models and underscores the influence of their respective configurations and forcings. After impacting the coast, the oil slick was pushed further southwest by currents (Fontana, 2018). As shown in Fig. 3, bottom-left, the simulations accurately exhibit the presence of particles along the French coast after the 20th of October, with event the CMEMS simulation showing particles arriving at the impact zone near Saint Tropez, albeit with a delay of many days than expected.

5.2. Oil spill dispersion with combined surface currents, wind and Stokes drift forcing from multiple models

The second scenario presents the integration of the 10-meter wind field and Stokes drift forcing to improve the understanding of dispersion driving processes. Data from the ERA5 and MeteOcean-UniGe models will be used in combination with the currents from CMEMS, SHOM and IFREMER leading to 6 different simulations. This approach is motivated by the significant differences in resolution between the two climate models, allowing a comparison of their results and providing a comprehensive view of the dispersion dynamics of the oil spill. We have divided this scenario into different sub-cases in order to evaluate the role of each forcing (currents, wind, waves) and their combination:

- Combined forcing of surface currents, 10-m wind field and Stokes drift
- Combined forcing of surface currents and 10-m wind field
- Combined forcing of surface currents and Stokes drift

5.2.1. Sea surface currents combined with wind field and Stokes drift forcing

The first sub-case represents the simulations with currents from the three ocean circulation models in combination with both 10-m wind field and Stokes drift forcing from ERA5 and MeteOcean-UniGe. For the MeteOcean-UniGe simulations, the northward and eastward velocities of Stokes drift are calculated using Eq. (2). The LPT model is forced by the combination of all three forcing following Eq. (1) where the β and α need to be evaluated. For this a sensitivity analysis has been carried out to find the optimal β and α based on the knowledge of the

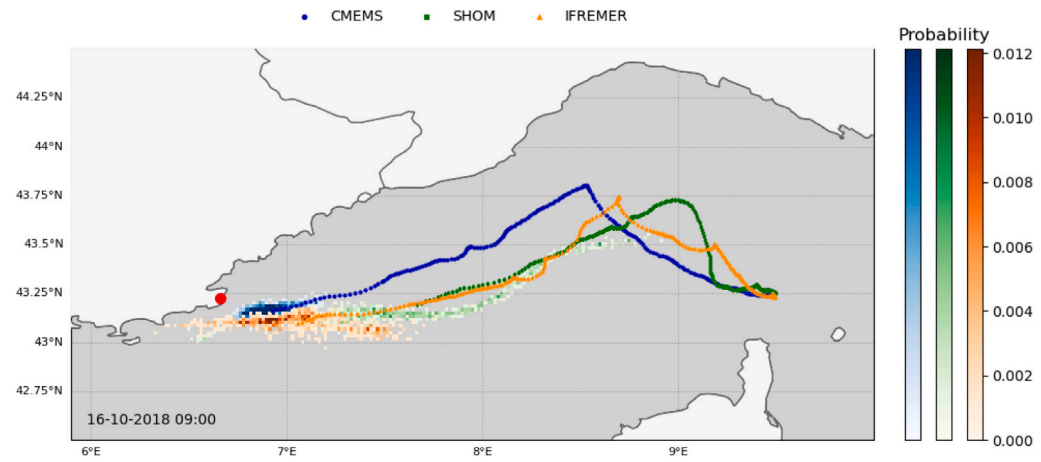

Fig. 4. Evolution of oil spills with relative probability for the three surface currents models (CMEMS, IFREMER and SHOM) in combination with ERA5 wind field and Stokes Drift forcing on the 16th October 2018 09:00. (For interpretation of the references to color in this figure legend, the reader is referred to the web version of this article.)

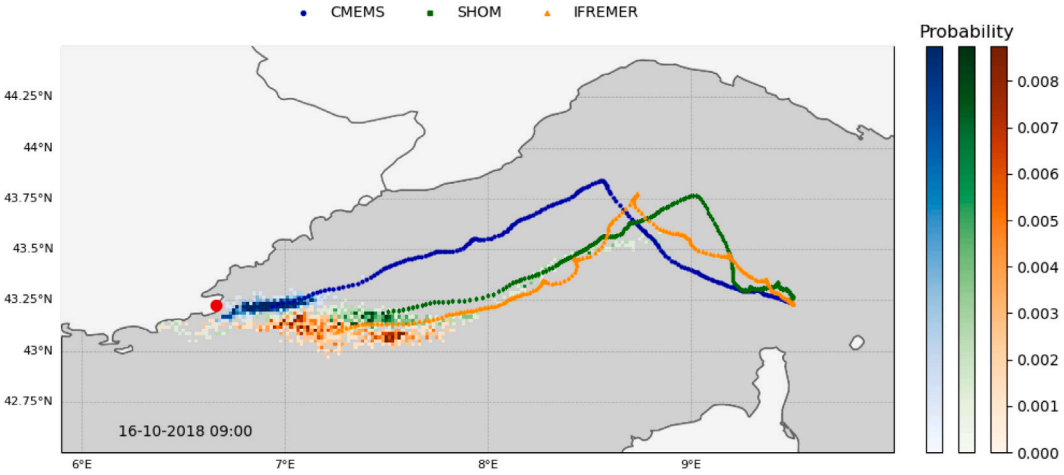

Fig. 5. Evolution of oil spills with relative probability for the three surface currents models (CMEMS, IFREMER and SHOM) in combination with MeteOcean-UniGe wind field and Stokes Drift forcing on the 16th October 2018 09:00. (For interpretation of the references to color in this figure legend, the reader is referred to the web version of this article.)

area and time-of-impact of the oil spill at the French coast. Initially, the same coefficients for α and β were used, specifically $\alpha = 0.3$ and $\beta = 0.02$ for the ERA5 and the MeteOcean-UniGe simulations for all three ocean model combinations. However, for the IFREMER model, it was necessary to adjust these coefficients in both scenarios to obtain a more reliable simulation, according to the only two evidences relating to the specific case study (i.e. the area of impact and satellite images). Consequently, for CMEMS and SHOM the original values, $\alpha = 0.3$ and $\beta = 0.02$ for ERA5 and MeteOcean-UniGe were maintained, while for IFREMER coefficients were changed to $\alpha = 0.3$ and $\beta = 0.03$ for the simulations in combination with ERA5 and MeteOcean-UniGe. The final α and β values are reported in Table 1. The coefficients are strongly influenced by the specific weather and sea conditions, seasonality and oil spill characteristics. Figs. 4 and 5 show the progressive trajectories of the oil slicks for the simulations of surface currents in combination with ERA5 and MeteOcean-UniGe, respectively. As observed, for both ERA5 and MeteOcean-UniGe there is a clear improvement, in terms of expected oil-spill trajectory, from the previous simulations that were forced with only sea surface currents.

The MeteOcean-UniGe model, which has a higher grid resolution than the ERA5 model, presents an improvement in the accuracy of the simulations with reduced particle diffusion and a slight better precision in predicting the impact area on the French coast as shown in Fig. 5. The three simulations maintain a certain difference between their trajectories, but the general trends are very similar to those shown in Fig. 4. With the introduction of the coefficients chosen according to each model, all the simulations arrive at the area of impact on the French coast on the same day and no longer on different dates as in the case of the simulations with currents alone. It is also worth noting that the CMEMS model, which in Fig. 3 shows a vortex at the height of the Ligurian coast, is no longer present in the two results in Figs. 4 and 5, which show a trajectory more similar to that of IFREMER and SHOM. Finally, it can be noted how the diffusion of the particles present in the case of the currents is no longer so marked in the results obtained by implementing the wind and Stokes drift, improving the achievement of the impact area where hydrocarbons were actually found on the French coast and not in other areas where this did not occur.

Table 1
α and β coefficients for the simulations.

	CMEMS	SHOM	IFREMER
α	0.3	0.3	0.3
β	0.02	0.02	0.03

To further evaluate the accuracy of the results, a comparison is conducted between the oil slick simulations and the SAR satellite

Table 2
Sentinel-I product IDs.

Image	Product ID
08/10/2018 07:28	S1A_IW_GRDH_1SDV_20181008T052757_20181008T052822_024040_02A081_CA4D
08/10/2018 19:21	S1B_IW_GRDH_1SDV_20181008T172145_20181008T172210_013064_01822C_B07F
09/10/2018 19:14	S1A_IW_GRDH_1SDV_20181009T171427_20181009T171452_024062_02A131_E887

Table 3
MeteOcean-UniGe model. P_{in} - Percentage of particles detected inside the oil slick area for each instant of the SAR images. $D_{centroid}$ - Distance between the centroids of particle dispersion simulations and the centroid of the observed SAR image.

Date and time		CMEMS	SHOM	IFREMER
08/10/2018 07:28	P_{in} [%]	12.50	3.38	5.00
	$D_{centroid}$ [km]	8.87	11.98	11.70
08/10/2018 19:21	P_{in} [%]	24.25	21.75	12.12
	$D_{centroid}$ [km]	8.38	13.56	9.39
09/10/2018 19:14	P_{in} [%]	38.12	15.75	7.38
	$D_{centroid}$ [km]	7.87	18.49	6.81

Table 4
ERA5 model. P_{in} - Percentage of particles detected inside the oil slick area for each instant of the SAR images. $D_{centroid}$ - Distance between the centroids of particle dispersion simulations and the centroid of the observed SAR image.

Date and time		CMEMS	SHOM	IFREMER
08/10/2018 07:28	P_{in} [%]	13.75	5.75	9.00
	$D_{centroid}$ [km]	8.17	11.36	11.15
08/10/2018 19:21	P_{in} [%]	13.25	25.87	12.38
	$D_{centroid}$ [km]	7.87	12.85	7.62
09/10/2018 19:14	P_{in} [%]	38.00	8.88	7.12
	$D_{centroid}$ [km]	8.37	19.53	9.92

images of the oil slick (Magrì et al., 2021). Specifically, the images of the Copernicus Sentinel-1 satellites with the product IDs reported in 2 are used.

All data are acquired from the (Sentinel Hub platform), which provides operational access to Sentinel-1 data in GRD mode with orthorectification and geometric correction applied. Radar images from the Sentinel-1 mission (Interferometric Wide Swath mode, GRD — Ground Range Detected, VV polarization) are used for the analysis. According to the (Copernicus SentiWiki platform), the orbital configuration of the Sentinel-1 constellation consists of two satellites Sentinel-1 A and Sentinel-1B and allows images of the same region to be acquired every 12 h. They operate on orbits offset by about 180° and cover the same area at intervals of about 6 days each, but by combining them it is possible, under certain orbital conditions and for certain regions, to obtain images of the same area at intervals of less than 24 h. Moreover, due to favorable weather conditions with wind speeds ranging from 2 to 10 m/s on 8 and 9 October, satellite images are made possible (Espedal and Wahl, 1999). Fig. 6 illustrates in the left panel three time instants at which the slick is detected by the satellite, represented by the red outline, in comparison with the simulations carried out with the three ocean circulation models surface currents in combination with MeteOcean-UniGe wind field and Stokes drift. The right panel shows the corresponding satellite images. It can be observed that although the speed of movement differs, the simulation derived from the CMEMS model is the one that most closely aligns with the actual slick points for MeteOcean-UniGe. As mentioned, the MeteOcean-UniGe simulations present a lower dispersion of the oil slick, in agreement with the satellite images.

The results, giving the distances between the centroids of the simulations and that of the satellite images (Eq. (10)) and the percentage of particles simulated for each model intersecting slicks detected by SAR (Eq. (11)), for the three temporal instants are reported in Table 3 and reveal variations in percentages across the models, reflecting their relative performance in simulating the spill dynamics. These variations are related to the input characteristics of each simulation as well as the introduced α and β coefficients, although these vary only for the β coefficient of 0.01 between models.

The results demonstrate that the CMEMS model is the most accurate in this analysis, exhibiting the minimal distances between centroids and the highest percentage of simulated particles within the temporal image area, in comparison to the outcomes from the SHOM and IFREMER models.

The same procedure is then applied to simulations obtained with Stokes drift and wind data from ERA5, compared with satellite images at the three times. Fig. 7 shows the results obtained, and what can be observed is a certain similarity in the trends of the models with the results obtained in Fig. 6.

Table 4 shows the data obtained for the distance between the centroid of the satellite image and the centroids of the three simulations, and the percentage of particles falling within the area of the SAR image. It can be noted that, compared to the results obtained for the case of MeteOcean-UniGe, the simulations generally perform slightly worse, with larger values of distance between the centroids and lower percentages of particles within the area of the satellite image. Even in this case, at the first three instances, it is the CMEMS model that gives overall the best results.

5.2.2. *Surface currents combined with wind field forcing*

Fig. 8 presents the results of the simulations forced with surface currents from the three ocean circulation models and wind field from ERA5. The coefficients used for the wind component, $\beta = 0.03$ for CMEMS and SHOM, while $\beta = 0.02$ for IFREMER, are the same as the one used in previous simulations. The results show that the slicks travel a significant distance when the wind forcing is introduced. The wind, in particular, appears to contribute significantly to advection, accelerating the movement of particles on the water surface and increasing the area affected compared to what is observed with surface currents alone. This highlights the importance of wind in determining the overall behavior and dispersion of particles on the water surface, as has already been demonstrated in others studies such as Prigent et al. (2017).

In this scenario, despite the low coefficient of wind, 2%–3%, its high magnitude nevertheless exerts a significant impact on the simulation. This is evidenced by Fig. 9, which compares the wind and Stokes drift magnitudes at a point in the simulation domain (43°12'18"N, 7°30'32"E). A difference in order of magnitude reaching $\sim O(10^2)$ between wind and Stokes drift is observed which reflects the contribution of wind in the oil spill evolution.

Fig. 10 presents the results of the simulations using surface currents from the three ocean models combined with wind field from the MeteOcean-UniGe model. The wind effect is applied with coefficients $\beta = 0.02$ for CMEMS and SHOM and $\beta = 0.03$ for IFREMER. The results indicate that the patches move a considerable distance when surface currents and wind are taken into account. However, with the chosen β, the calculated speed of movement is higher than that observed in the case study, i.e. the particles arrive sooner at the French coast than the

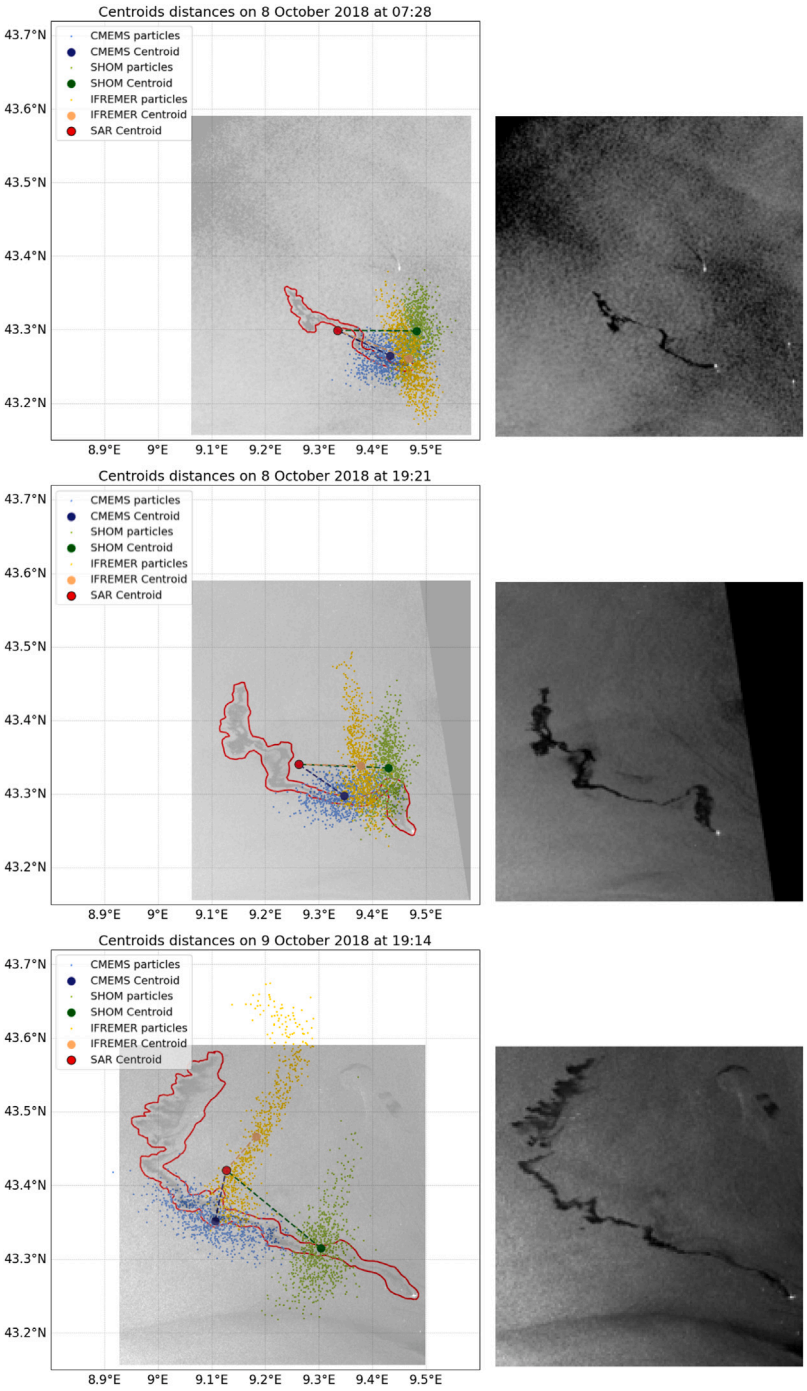

Fig. 6. Left panel — Oil slicks trajectories simulated with three sea water velocity models in combination with Stokes drift and wind field forcing from MeteOcean-UniGe compared with SAR images from Copernicus Sentinel-1 at three different times (red outlines). Right panel — Corresponding satellite images, from top to bottom, 08/10/2018 at 7:28, 08/10/2018 at 19:21, 09/10/2018 at 19:14. (For interpretation of the references to color in this figure legend, the reader is referred to the web version of this article.)

expected impact date of 16/10/2018. Despite the lower coefficient, the impact of wind is substantial due to its magnitude (Fig. 9), contributing to the greater dispersion and rapid movement of particles on the water surface. It can be observed that the introduction of the wind component results in trajectories with a comparable overall trend across the three simulations, despite exhibiting differences in the reversal point from north-west to south-west. It is also of interest to note that the trajectory trends for the MeteOcean-UniGe model (Fig. 10) and ERA5 (Fig. 8) are rather similar, differing only in the speed at which the particles move towards the area of impact, with the MeteOcean-UniGemodel exhibiting a faster rate of movement than ERA5.

5.2.3. *Surface currents combined with Stokes drift forcing*

Figs. 11 and 12 illustrate the results of the simulations forced with the sea surface currents (CMEMS, SHOM and IFREMER) in combination

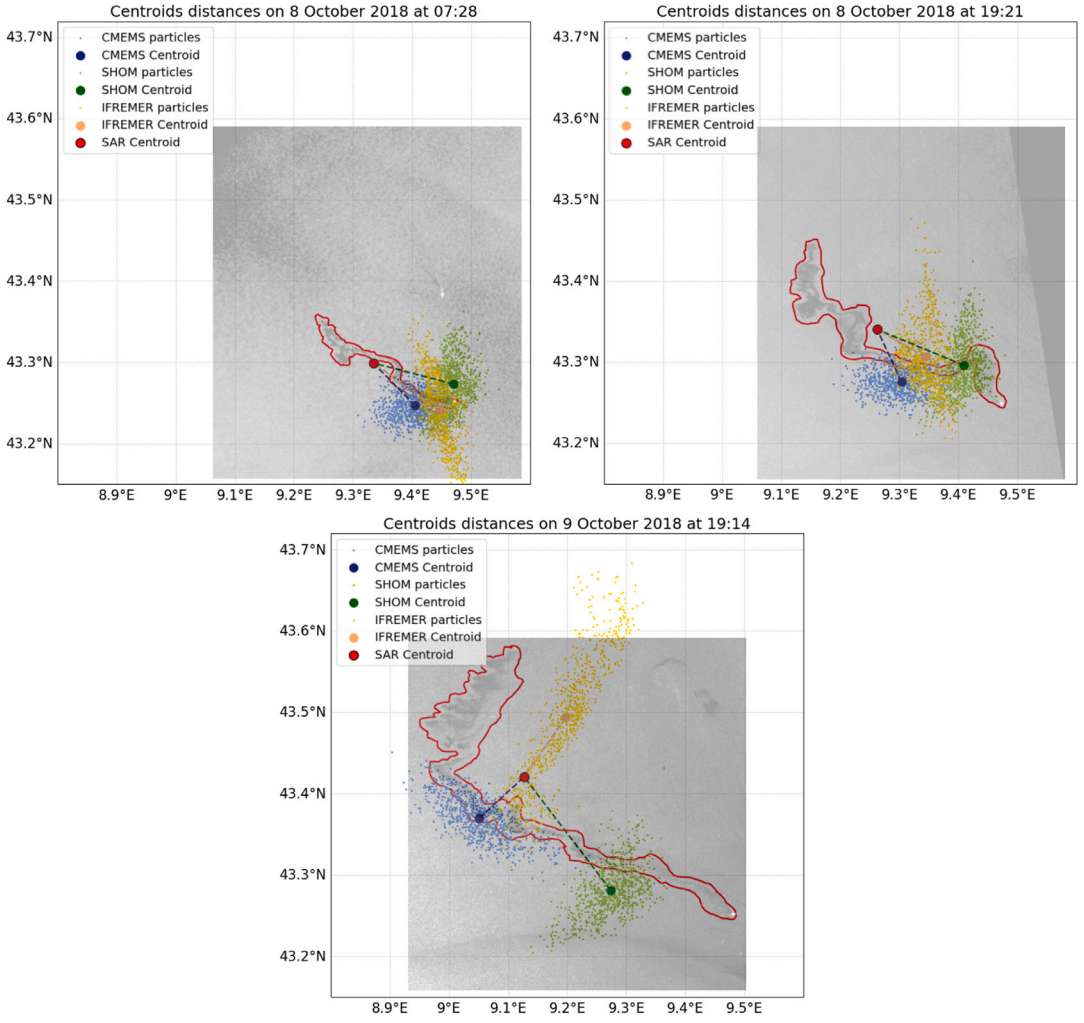

Fig. 7. Oil slicks trajectories simulated with three sea water velocity models in combination with Stokes drift and wind field forcing from ERA5 model, compared with SAR images from Copernicus Sentinel-1 at three different times (red outlines). On the upper left, the 08/10/2018 at 7:28, in the upper right the 08/10/2018 at 19:21. and on the bottom, the position of 09/10/2018 at 19:14. (For interpretation of the references to color in this figure legend, the reader is referred to the web version of this article.)

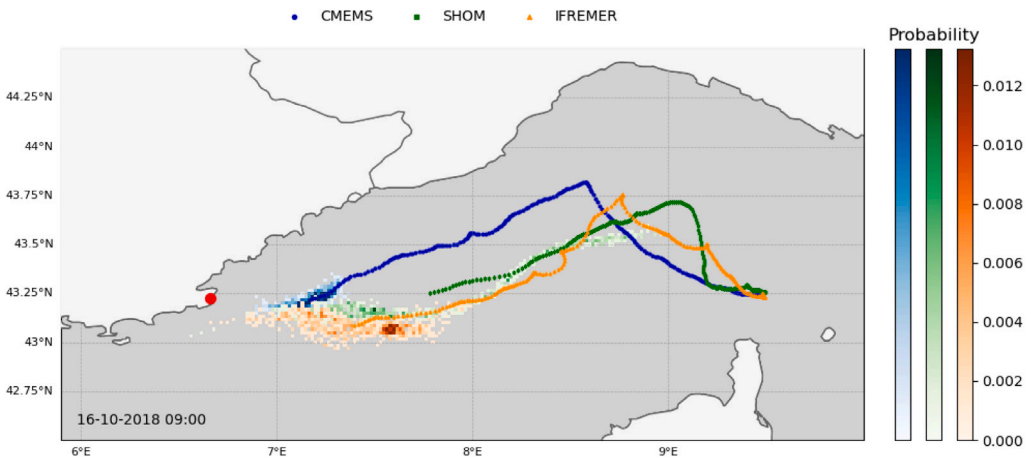

Fig. 8. Evolution of oil spills with relative probability for the three surface currents models (CMEMS, IFREMER and SHOM) in combination with ERA5 wind field forcing on the 16th October 2018 09:00. (For interpretation of the references to color in this figure legend, the reader is referred to the web version of this article.)

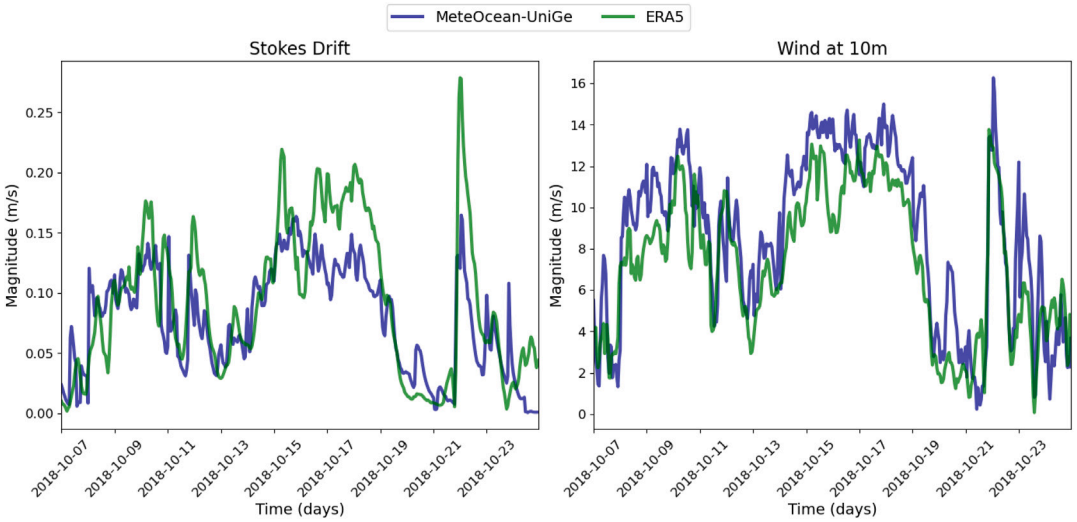

Fig. 9. Comparison of the magnitude of Wind and Stokes drift for both ERA5 and MeteOcean-UniGe at the location of coordinates 43°12'18"N, 7°30'32"E. (For interpretation of the references to color in this figure legend, the reader is referred to the web version of this article.)

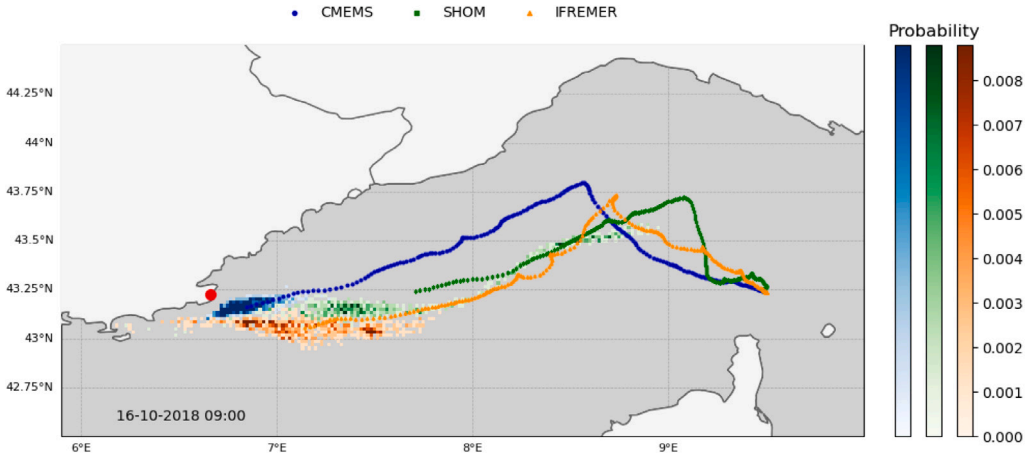

Fig. 10. Evolution of oil spills with relative probability for the three surface currents models (CMEMS, IFREMER and SHOM) in combination with MeteOcean-UniGe wind field forcing on the 16th October 2018 09:00. (For interpretation of the references to color in this figure legend, the reader is referred to the web version of this article.)

with the Stokes drift induced by waves from ERA5 and MeteOcean-UniGe with $\alpha = 0.3$ for both the ERA5 and the MeteOcean-UniGe simulations.

From Figs. 11 and 12, it is evident that the simulated trajectory differs significantly from what was observed in the previous results, where the wind component was considered. In this scenario, the Stokes drift component has a minimal impact on the advection process, whereas it contributes more in the general spatial distribution of the simulated spill. It is evident that the outputs of the current analysis exhibit a similarity to those obtained in previous simulations utilizing only the sea surface currents in paragraph Section 5.1. This is a consequence of the low value of the α coefficient employed in the present analysis. The output of the MeteOcean-UniGe and ERA5 simulations demonstrates a high correlation in the trajectories of the simulations, with the primary distinction being in the diffusion of the particles. As illustrated in the ERA5 Fig. 11, the CMEMS model simulation exhibits a notable divergence in particle diffusion compared to the results obtained with the MeteOcean-UniGe model simulations (Fig. 12).

5.3. Mixing properties

A comparative analysis of the different mixing properties described in Section 3.2 is presented for the simulations carried out with the forcing combination of surface currents, wind and Stokes drift. Figs. 13 and 14 present the relative dispersion R^2, the absolute distance D_{b0} and the relative distance D_b, for the simulations carried out with the different forcing combinations of currents and ERA5 wind and Stokes drift. The graphs in Fig. 13 indicate the total R^2 dispersion, and the two, x and y, components. A general trend of increasing dispersion over time is observed across all simulations in the three graphs. Notably, in the simulations that incorporate the wind and Stokes Drift factor in the bottom graph, there is a reduction in dispersion by almost an order of magnitude. This indicates that the two factors have a greater impact on particle advection than on particle dispersion.

In accordance with the data presented in Figs. 14, it is evident that the absolute distance is consistently less than the relative distance. This is due to the fact that the absolute distance only accounts for the linear distance between the initial and final centroids, whereas the relative distance considers the entire path traced by the virtual particles. As

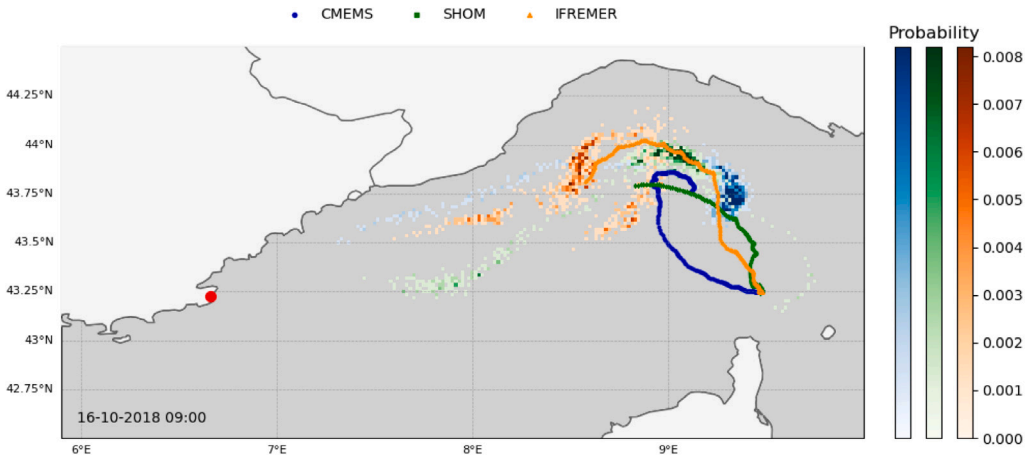

Fig. 11. Evolution of oil spills with relative probability for the three surface currents models (CMEMS, IFREMER and SHOM) in combination with ERA5 Stokes Drift forcing on the 16th October 2018 09:00. (For interpretation of the references to color in this figure legend, the reader is referred to the web version of this article.)

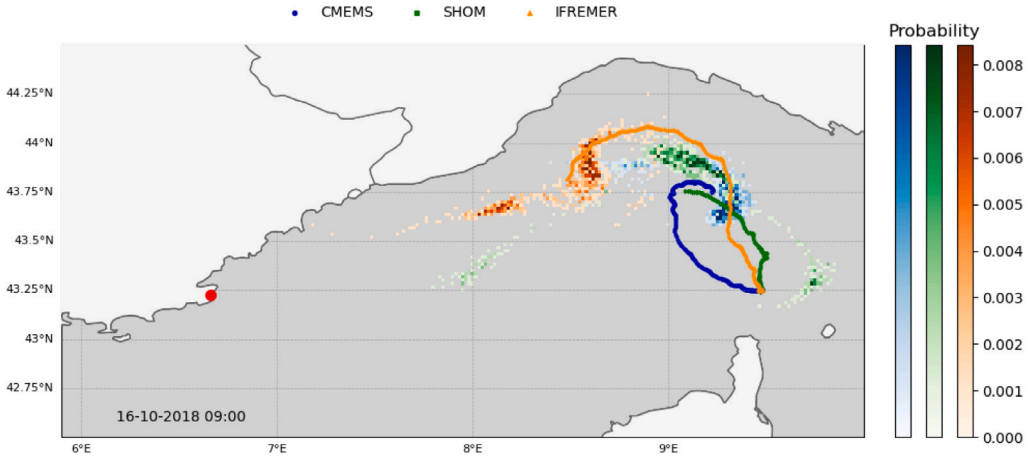

Fig. 12. Evolution of oil spills with relative probability for the three surface currents models (CMEMS, IFREMER and SHOM) in combination with MeteOcean-UniGe Stokes Drift forcing on the 16th October 2018 09:00. (For interpretation of the references to color in this figure legend, the reader is referred to the web version of this article.)

previously evidenced in the results obtained in paragraph Section 5.2, the output for the case where sea surface velocity and Stokes drift are considered exhibits a trajectory for the three simulations that is half in value that of the simulation with wind contribution. This is also evident in Fig. 14, which illustrates the results for the sea surface velocity with the Stokes drift contribution in the top panel. These results reach a maximum distance of 170 km for the IFREMER model. The results obtained for the graph on the top and on the bottom present a reaching distance of the trajectory of approximately 300 km, which is almost twice the result obtained in the graph with sea surface velocity and Stokes drift contribution.

Similar trends are observed in the results obtained by MeteOcean-UniGe where Fig. 15 represents the relative dispersion and the two components in x and y in the three cases of sea surface velocity, wind and Stokes drift. It can be observed that in all graphs, dispersion occurs gradually, increasing with time. It is interesting to note that the middle and bottom graphs show clear variations between the different simulations, with differences of more than an order of magnitude between the CMEMS and SHOM models.

Fig. 16 presents graphical representations of the absolute and relative distances for the various combinations of simulations. Furthermore, the results obtained with the MeteOcean-UniGe model demonstrate that the graphs illustrating sea surface velocity and wind (middle panel) and sea surface velocity, wind and Stokes drift (bottom panel) exhibit a similar trend to the graphs in Fig. 14. In particular, the graph representing sea surface velocity and Stokes drift reaches a distance of 175 km with the IFREMER model, while the other two graphs reach a distance of almost 300 km.

The graphs in Figs. 17 and 18 depict the Probability Density Function (PDF) of the dispersion R^2 estimated at four time intervals, for every model, resulting in nine different lines in each graph. The PDF is then estimated numerically by counting how many particles fall within predefined intervals (bins) of R^2 and normalizing the counts so that the area under the curve equals one.

The Figs. 17 and 18, respectively, are derived from the ERA5 and MeteOcean-UniGe results and represent the probability density function of the relative dispersion in the three cases for each model simulation. The graphs illustrate the temporal evolution of the simulation at three distinct points in time. It is evident that in the period surrounding the release date, the probability density function (PDF) is higher than it is many days later, where the PDF becomes lower and more elongated. This phenomenon is reflected in the PDF graphs, which demonstrate that the particle cloud initially remains compact and then gradually expands over time.

6. Conclusions

This study highlights the considerable variability between oceanographic and climate models used to simulate the dispersion of oil spills

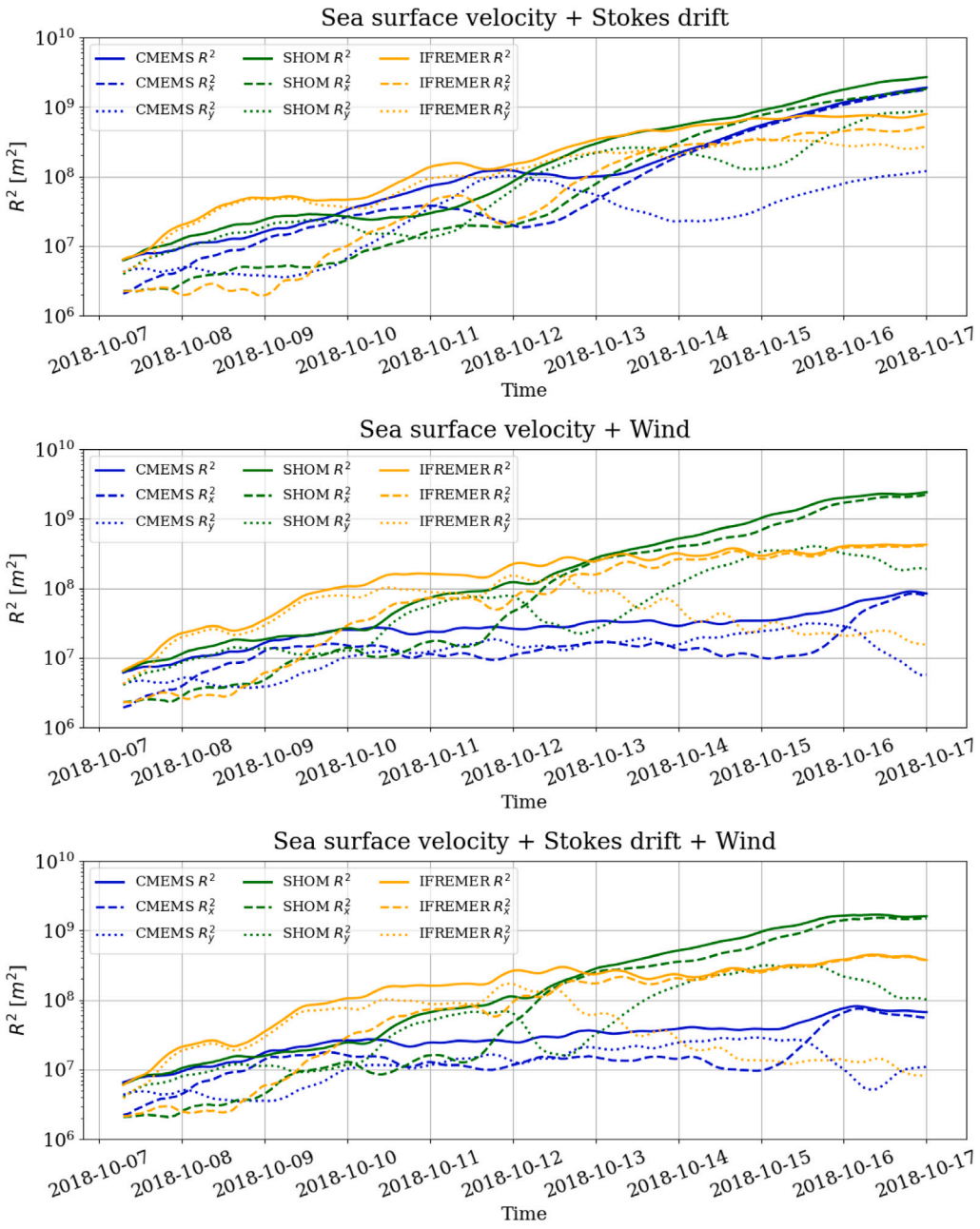

Fig. 13. ERA5 Model — The graphs represent respectively the relative dispersion (continuous line) of the three models with bilogarhythmic trend and dispersion in x-direction (dashed line) and y-direction (dotted line). (For interpretation of the references to color in this figure legend, the reader is referred to the web version of this article.)

in the Mediterranean Sea. This work focused on the simulation of trajectories and dispersion patterns for different input current, wind and wave models, proving that even minor variations in model parameters, initial conditions, or spatial resolution can lead to significant differences in the obtained dispersion results, highlighting the need for careful model selection and calibration to improve prediction accuracy. Dispersion analysis for all model combinations is carried out using identical particle release setup. A sensitivity analysis regarding particle release spread and density could improve the understanding of further insights regarding trajectories linked to the dispersion model parameterizations. Despite these differences, all models generally predict a westward movement towards the French coast, although the timing and magnitude of the impacts vary. The crucial role of environmental factors such as wind speed and Stokes drift in improving the realism and accuracy of dispersion simulations is highlighted. Wind-induced transport, which results from friction between the wind and the ocean surface, significantly accelerates and expands the dispersion of oil slicks, creating strong surface currents that effectively disperse pollutants over greater distances. In contrast, Stokes drift, a consequence of wave motion in which water particles move in circular or elliptical orbits, contributes modestly to the transport of pollutants, particularly in areas of high wave activity. Although Stokes drift can influence the distribution of floating pollutants, in this scenario it is less important than wind-induced transport, which generates more significant advection and broader distribution patterns. Despite Stokes drift coefficients can be higher, the greater magnitude of wind speeds exerts a more dominant influence on dispersion predictions, highlighting the importance of understanding both coefficients. Wave action can also lead to vertical entrainment of oil droplets into the water column, a process not included in this 2D approach. Effective calibration of

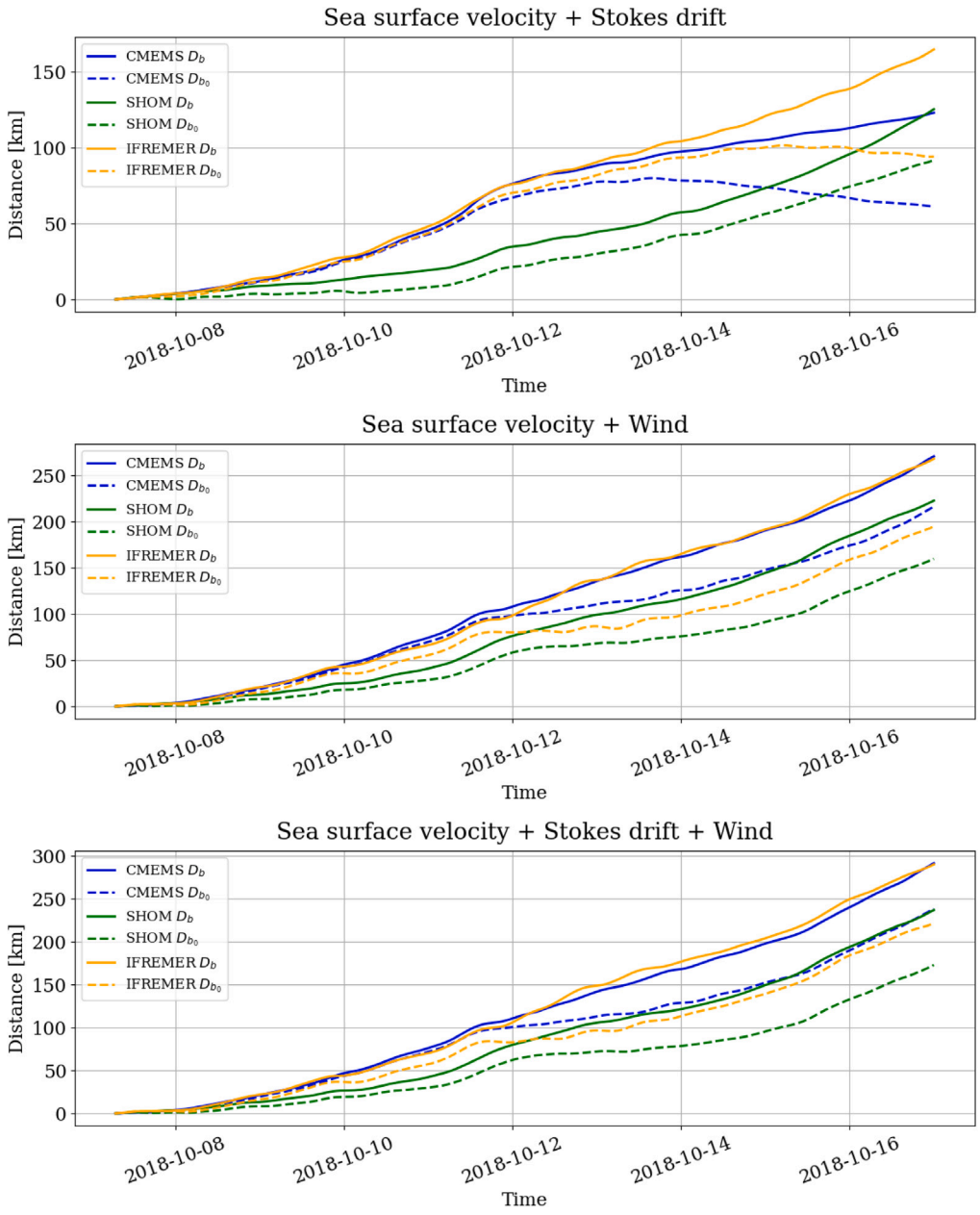

Fig. 14. ERA5 Model — The graphs show the relative distance D_b (continuous line) and the absolute distance D_{b0} (dashed line) related to the three models. Top panel: results for sea surface velocity and Stokes drift contribution; Middle panel: results for sea surface velocity and wind component; Bottom panel: results for sea surface velocity, wind and stokes drift contributions. (For interpretation of the references to color in this figure legend, the reader is referred to the web version of this article.)

model coefficients, including those for Stokes drift (α) and wind effects (β), is essential to optimize simulation accuracy. In this study, due to the lack of precise and detailed observations of the spill's evolution and/or the exact point and time of impact, a qualitative approach was adopted to determine the optimal parameters, providing an estimate of the cloud's position near the impact area and the expected date. When detailed observations are available, the methodology presented here can be significantly improved by conducting a systematic optimization approach (e.g. Bayesian optimization). Despite the fact that the SHOM model used in this study is based on archived forecast data rather than reanalysis products, the results it produced are remarkably similar to those of the CMEMS and IFREMER models when integrated with wind and wave forcings. This consistency indicates that the SHOM forecast model can be used alongside other reanalyses products for multi-model ensemble analysis such as the one presented in this work. The ability of the model to produce results consistent with reanalysis-based models, despite its predictive nature, underscores its reliability for predictive applications. This finding is particularly relevant for scenarios where reanalysis products may not be immediately available, highlighting the potential of SHOM as a robust and operationally viable model for real-time decision making in oil spill response. The Corsican oil spill case study illustrates the practical implications of these findings, providing insights into the likely impact zones and temporal evolution of oil slicks that are valuable for emergency response and containment strategies. The findings of this study highlight the necessity for the development of highly accurate and flexible simulation tools in the context of oil spill

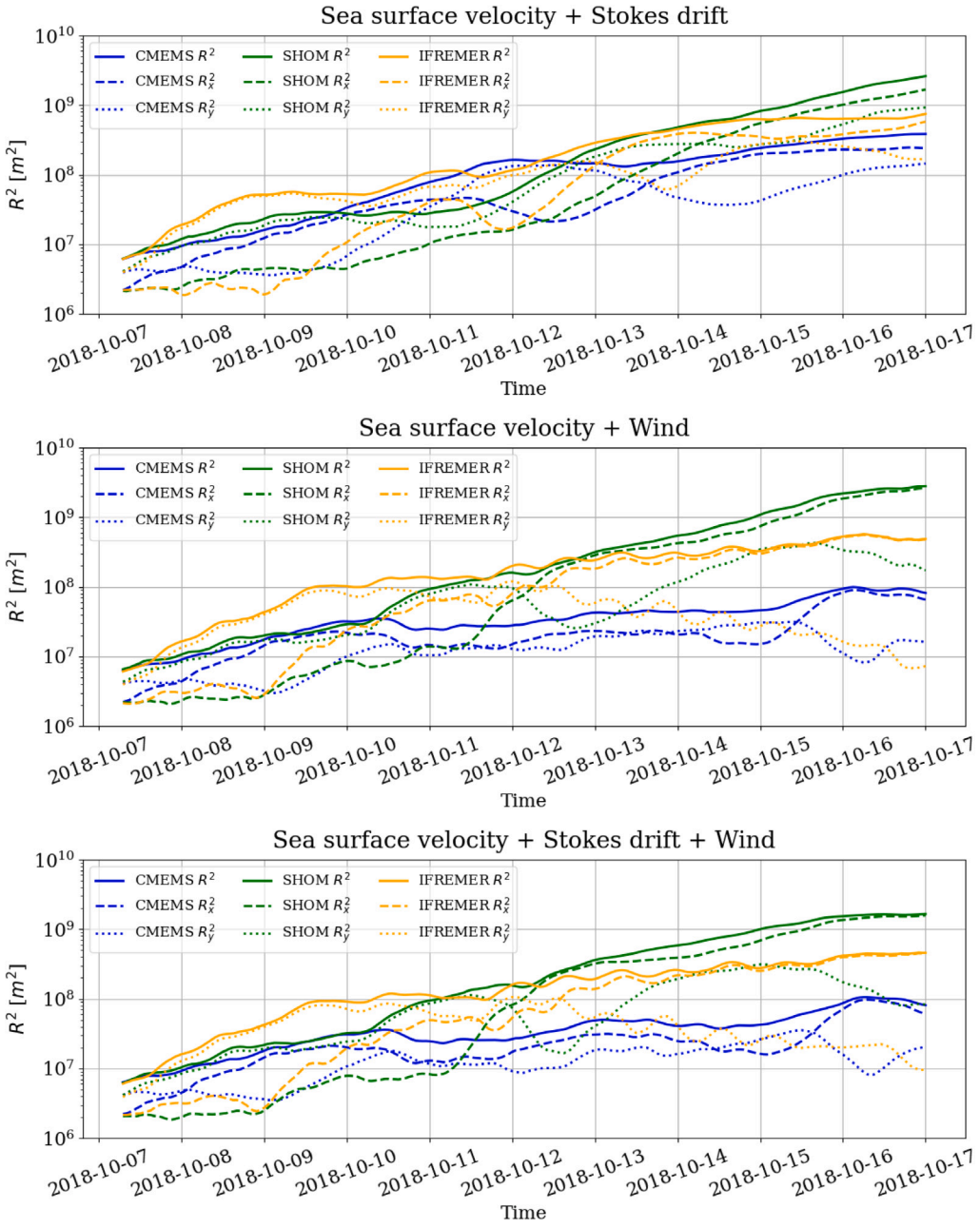

Fig. 15. MeteOcean-UniGe Model — The graphs represent respectively the relative dispersion (continuous line) of the three models with bilogarhythmic trend and dispersion in x-direction (dashed line) and y-direction (dotted line). (For interpretation of the references to color in this figure legend, the reader is referred to the web version of this article.)

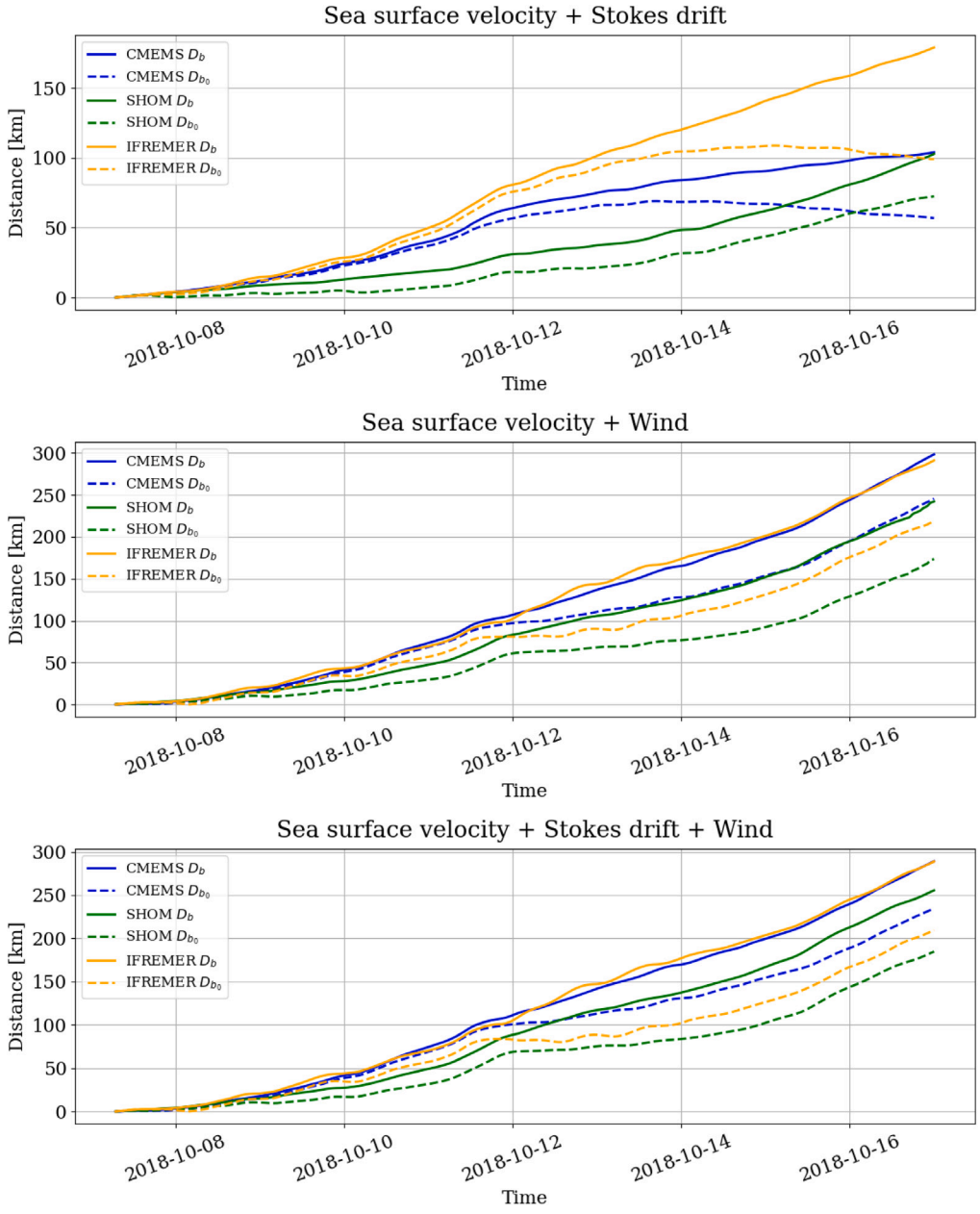

Fig. 16. MeteOcean-UniGe Model — The graphs show the relative distance D_b (continuous line) and the absolute distance D_{b0} (dashed line) related to the three models. Top panel: results for sea surface velocity and Stokes drift contribution; Middle panel: results for sea surface velocity and wind component; Bottom panel: results for sea surface velocity, wind and stokes drift contributions. (For interpretation of the references to color in this figure legend, the reader is referred to the web version of this article.)

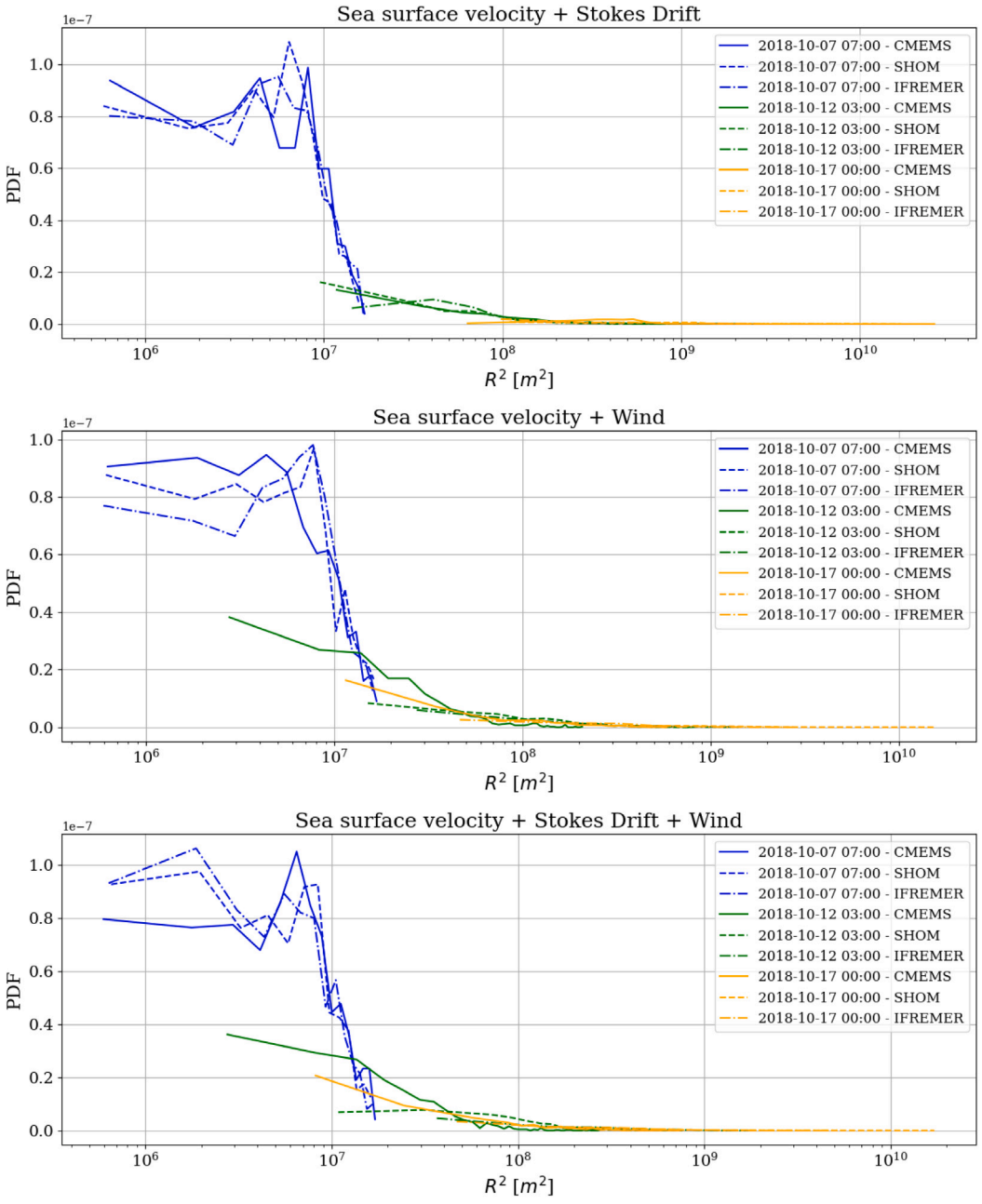

Fig. 17. ERA5 Model — representation of probability density function (PDF) of R^2 in three different instants of time. (For interpretation of the references to color in this figure legend, the reader is referred to the web version of this article.)

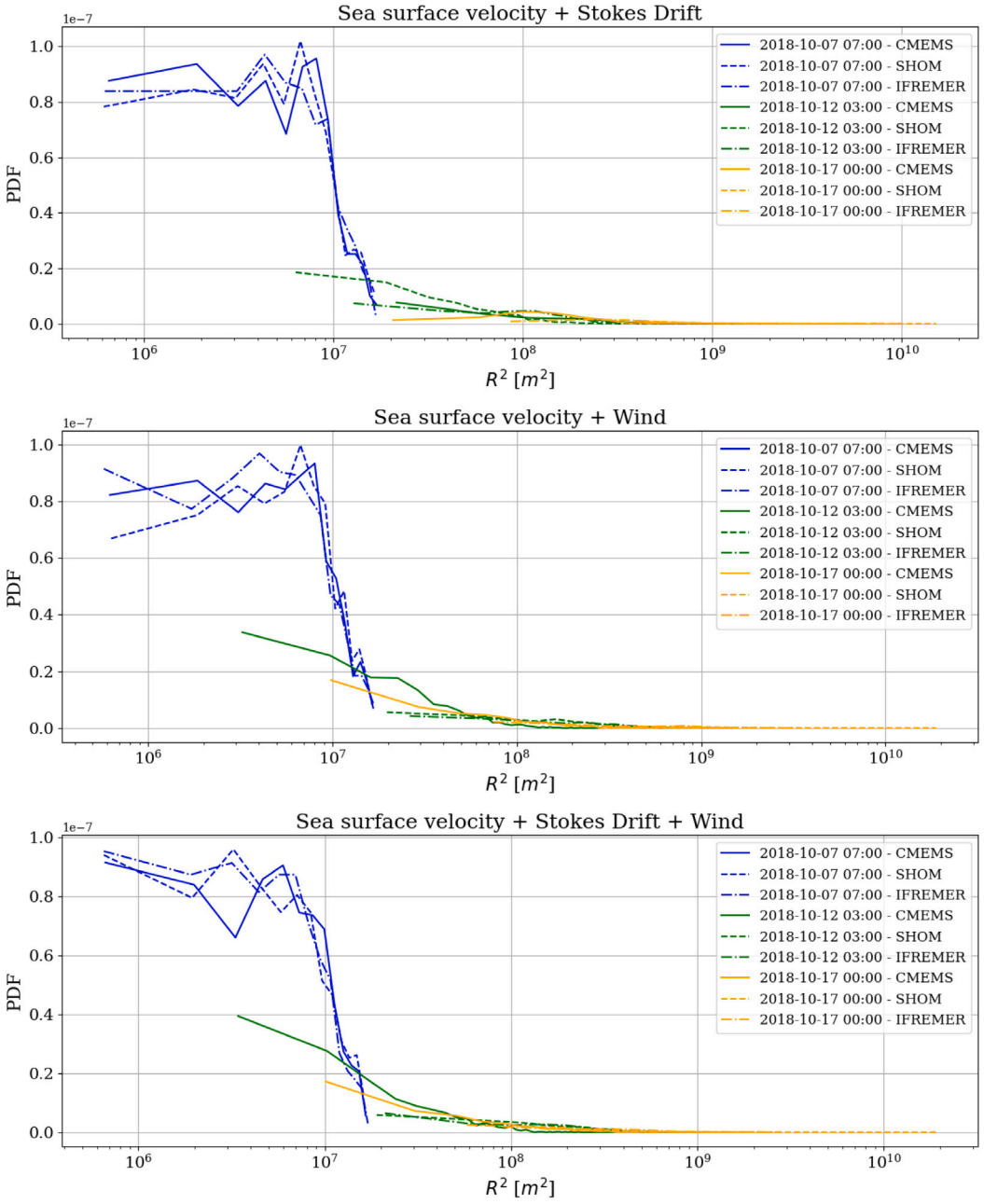

Fig. 18. MeteOcean-UniGe Model — representation of probability density function (PDF) of R^2 in three different instants of time. (For interpretation of the references to color in this figure legend, the reader is referred to the web version of this article.)

management and prevention activities. The demonstrated variability among oceanographic and climate models emphasizes the importance of rigorous model selection, calibration and validation procedures to ensure the reliability of the resulting predictions. The incorporation of key environmental forcings, such as wind speed and Stokes drift, enhances the capacity to anticipate the evolution of oil spills, enabling authorities to implement timely and effective response measures. The insights gained, particularly through the Corsican case study, indicate the potential to optimize containment and mitigation efforts, safeguard fragile ecosystems like the Pelagos Sanctuary, and improve preparedness for future maritime incidents. This study demonstrates the direct benefits of developing ocean forecasting systems and improving the accuracy of predictions.

CRediT authorship contribution statement

Beatrice Maddalena Scotto: Writing – review & editing, Writing – original draft, Visualization, Validation, Software, Resources, Methodology, Formal analysis, Data curation, Conceptualization. **Andrea Lira Loarca:** Writing – review & editing, Supervision, Methodology, Conceptualization. **Antonio Novellino:** Writing – review & editing, Supervision, Resources. **Giovanni Besio:** Writing – review & editing, Supervision, Resources, Project administration, Methodology, Conceptualization.

Declaration of competing interest

The authors declare that they have no known competing financial interests or personal relationships that could have appeared to influence the work reported in this paper.

Acknowledgments

B.M.S. is supported by a grant within the framework of the REGIONAL PROGRAMME EUROPEAN SOCIAL FUND+ 2021-2027 PRIORITY 2 - EDUCATION AND TRAINING - ESO 4.6 (OS-f) in collaboration with and with the contribution of ETT S.p.A. (NextGenerationEU and MUR, NRRP project Robotics and AI for Socio-economic Empowerment, RAISE, no.ECS00000035; Ocean observations and indicators for climate and assessments, ObsSea4Clim, Grant agreement ID: 101136548, 10.3030/101136548 Internal contribution Nr. 22).

Data availability

Data will be made available on request.

References

Abascal, A., Castanedo, S., Mendez, F., Medina, R., Losada, I., 2009. Calibration of a Lagrangian transport model using drifting buoys deployed during the prestige oil spill. J. Coast. Res. 25, http://dx.doi.org/10.2112/07-0849.1.

Abernathey, R., Gnanadesikan, A., Pradal, M.-A., Sundermeyer, M.A., 2022. Chapter 9 - Isopycnal mixing. In: Meredith, M., Naveira Garabato, A. (Eds.), Ocean Mixing. Elsevier, pp. 215–256. http://dx.doi.org/10.1016/B978-0-12-821512-8.00016-5.

Ardhuin, F., Rogers, E., Babanin, A., Filipot, O., Magne, R., Roland, A., Van, A., Westhuysen, D., Queffeulou, P., Lefevre, J.-M., Aouf, L., Collard, F., 2010. Semiempirical dissipation source functions for ocean waves. Part I: Definition, calibration, and validation. J. Phys. Oceanogr. 40, 1917. http://dx.doi.org/10.1175/2010JPO4324.1.

Beegle-Krause, C., 2001. General NOAA oil modeling environment (GNOME): A new spill trajectory model. Int. Oil Spill Conf. Proc. 2001, http://dx.doi.org/10.7901/2169-3358-2001-2-865.

Berry, A., Dabrowski, T., Lyons, K., 2012. The oil spill model OILTRANS and its application to the celtic sea. Marine Poll. Bull. (ISSN: 0025-326X) 64 (11), 2489–2501. http://dx.doi.org/10.1016/j.marpolbul.2012.07.036, URL https://www.sciencedirect.com/science/article/pii/S0025326X12003578.

Berta, M., Bellomo, L., Magaldi, M.G., Griffa, A., Molcard, A., Marmain, J., Borghini, M., Taillandier, V., 2014. Estimating Lagrangian transport blending drifters with HF radar data and models: Results from the TOSCA experiment in the ligurian current (north western mediterranean sea). Prog. Oceanogr. 128, 15–29. http://dx.doi.org/10.1016/j.pocean.2014.08.004.

Besio, G., Mentaschi, L., Mazzino, A., 2016. Wave energy resource assessment in the mediterranean sea on the basis of a 35-year hindcast. Energy (ISSN: 0360-5442) 94, 50–63. http://dx.doi.org/10.1016/j.energy.2015.10.044, URL https://www.sciencedirect.com/science/article/pii/S0360544215014127.

Cao, R., Chen, H., Rong, Z., Lv, X., 2021. Impact of ocean waves on transport of underwater spilled oil in the bohai sea. Marine Poll. Bull. (ISSN: 0025-326X) 171, 112702. http://dx.doi.org/10.1016/j.marpolbul.2021.112702, URL https://www.sciencedirect.com/science/article/pii/S0025326X21007360.

Cassola, F., Ferrari, F., Mazzino, A., Miglietta, M., 2016. The role of the sea on the flash floods events over liguria (northwestern Italy). Geophys. Res. Lett. 43, n/a–n/a. http://dx.doi.org/10.1002/2016GL068265.

CEDRE, 2019. CSL virginia. URL https://wwz.cedre.fr/en/Resources/Spills/Spills/CSL-Virginia.

Dagestad, K.-F., Röhrs, J., Breivik, O., Ådlandsvik, B., 2018. OpenDrift v1.0: a generic framework for trajectory modelling. Geosci. Model. Dev. 11, 1405–1420. http://dx.doi.org/10.5194/gmd-11-1405-2018.

De Dominicis, M., Pinardi, N., Zodiatis, G., 2013. MEDSLIK-II, a Lagrangian marine oil spill model for short-term forecasting–part 1: Theory. Geosci. Model. Dev. 6, 1851–1869. http://dx.doi.org/10.5194/gmd-6-1851-2013.

Deandreis, M., Panaro, A., Ferrara, O., 2022. Maritime Scenario in the Mediterranean: Analysis of the Competitiveness and Investments of the Major Logistics Players. Istituto Affari Internazionali (IAI) Rome, Italy.

Escudier, R., Clementi, E., Omar, M., Cipollone, A., Pistoia, J., Aydogdu, A., Drudi, M., Grandi, A., Lyubartsev, V., Lecci, R., Cretí, S., Masina, S., Coppini, G., Pinardi, N., 2020. Mediterranean sea physical reanalysis (CMEMS MED-currents) (version 1) [data set]. Copernic. Monit. Environ. Mar. Serv. (CMEMS) http://dx.doi.org/10.25423/CMCC/MEDSEA_MULTIYEAR_PHY_006_004_E3R1.

Espedal, H.A., Wahl, T., 1999. Satellite SAR oil spill detection using wind history information. Int. J. Remote Sens. 20 (1), 49–65. http://dx.doi.org/10.1080/014311699213596.

EUROSTAT, 2024. Eurostat, maritime transport statistics - short sea shipping of goods. URL https://ec.europa.eu/eurostat/statistics-explained/index.php?title=Maritime_transport_statistics_-_short_sea_shipping_of_goods.

Ferrari, F., Besio, G., Cassola, F., Mazzino, A., 2020. Optimized wind and wave energy resource assessment and offshore exploitability in the mediterranean sea. Energy (ISSN: 0360-5442) 190, 116447. http://dx.doi.org/10.1016/j.energy.2019.116447, URL https://www.sciencedirect.com/science/article/pii/S0360544219321425.

Fontana, J.-B., 2018. Les plages de ramatuelle, saint tropez et sainte maxime souillées par des galettes de pétrole. FREQUENCE Sud.Fr URL https://www.frequence-sud.fr/art-59085-les_plages_de_ramatuelle__saint_tropez_et_sainte_maxime_souillees_par_des_galettes_de_petrole_ramatuelle.

Fossi, M.C., Panti, C., Marsili, L., Maltese, S., Spinsanti, G., Casini, S., Caliani, I., Gaspari, S., Muñoz-Arnanz, J., Jimenez, B., Finoia, M.G., 2013. The pelagos sanctuary for mediterranean marine mammals: Marine protected area (MPA) or marine polluted area? The case study of the striped dolphin (stenella coeruleoalba). Marine Poll. Bull. (ISSN: 0025-326X) 70 (1), 64–72. http://dx.doi.org/10.1016/j.marpolbul.2013.02.013.

Furuichi, N., Hibiya, T., 2015. Assessment of the upper-ocean mixed layer parameterizations using a large eddy simulation model. J. Geophys. Res.: Ocean. 120, 2350–2369. http://dx.doi.org/10.1002/2014JC010665.

Garnier, V., Pairaud, I., Nicolle, A., Alekseenko, E., Baklouti, M., Thouvenin, B., Lecornu, F., Garreau, P., 2014. MENOR: A HIGH-resolution (1.2 KM) MODELING OF THE NORTH-western mediterranean SEA ROUTINELY RUN BY THE PREVIMER operational FORECAST SYSTEM. Mercator-Ocean Newsl..

Hersbach, H., Bell, B., Berrisford, P., Hirahara, S., Horányi, A., Muñoz-Sabater, J., Thépaut, J.N., 2020. The ERA5 global reanalysis. Q. J. R. Meteorol. Soc. 146 (730), 1999–2049.

Hulianytskyi, A., 2022. Subdiffusion equations with a source term and their extensions. Rep. Math. Phys. (ISSN: 0034-4877) 89 (1), 1–8. http://dx.doi.org/10.1016/S0034-4877(22)00007-6.

IEA, 2023. International energy agency (IEA) 2023 suez canal - factsheet. URL https://iea.blob.core.windows.net/assets/0a3c8da7-43ad-4511-a0ff-932fd8d0825a/SuezCanal-Factsheet.pdf.

Kumar, N., Cahl, D., Crosby, S., Voulgaris, G., 2017. Bulk vs. Spectral wave parameters: Implications on Stokes drift estimates, regional wave modeling, and HF radars applications. J. Phys. Oceanogr. 47, http://dx.doi.org/10.1175/JPO-D-16-0203.1.

Lacasce, J., Mahadevan, A., 2006. Estimating subsurface horizontal and vertical velocities from sea-surface temperature. J. Mar. Res. 64, 695–721. http://dx.doi.org/10.1357/002224006779367267.

Lira-Loarca, A., Cáceres-Euse, A., De-Leo, F., Besio, G., 2022. Wave modeling with unstructured mesh for hindcast, forecast and wave hazard applications in the mediterranean sea. Appl. Ocean Res. (ISSN: 0141-1187) 122, 103118. http://dx.doi.org/10.1016/j.apor.2022.103118, URL https://www.sciencedirect.com/science/article/pii/S0141118722000694.

Lyubartseva, S., De Dominicis, M., Oddo, P., Coppini, G., Nadia, P., Greggio, N., 2015. Oil spill hazard from dispersal of oil along shipping lanes in the southern adriatic and northern ionian seas. Marine Poll. Bull. 90, 259–272. http://dx.doi.org/10.1016/j.marpolbul.2014.10.039.

Magrì, S., Vairo, T., Reverberi, A., Fabiano, B., 2021. Oil spill identification and monitoring from sentinel-1 sar satellite earth observations: a machine learning approach. Chem. Eng. Trans. 86, 379–384. http://dx.doi.org/10.3303/CET2186064.

Mentaschi, L., Besio, G., Cassola, F., Mazzino, A., 2013. Developing and validating a forecast/hindcast system for the mediterranean sea. J. Coast. Res. 65, http://dx.doi.org/10.2112/SI65-262.1.

Mentaschi, L., Besio, G., Cassola, F., Mazzino, A., 2015. Performance evaluation of wavewatch III in the mediterranean sea. Ocean. Model. (ISSN: 1463-5003) 90, 82–94. http://dx.doi.org/10.1016/j.ocemod.2015.04.003, URL https://www.sciencedirect.com/science/article/pii/S1463500315000578.

Míguez, B.M., Novellino, A., Vinci, M., Claus, S., Calewaert, J.-B., Vallius, H., Schmitt, T., Pititto, A., Giorgetti, A., Askew, N., Iona, S., Schaap, D., Pinardi, N., Harpham, Q., j. Kater, B., Populus, J., She, J., Palazov, A.V., McMeel, O., Oset, P., Lear, D., Manzella, G.M., Gorringe, P., Simoncelli, S., Larkin, K., Holdsworth, N., Arvanitidis, C.D., Jack, M.E.M., Montero, M.C., Herman, P.M., Hernandez, F., 2019. The European marine observation and data network (emodnet). Front. Mar. Sci http://dx.doi.org/10.3389/fmars.2019.00313.

Millot, C., Taupier-Letage, I., 2005. Circulation in the mediterranean sea. In: Saliot, A. (Ed.), The Mediterranean Sea. Springer Berlin Heidelberg, Berlin, Heidelberg, pp. 29–66. http://dx.doi.org/10.1007/b107143.

Moore, A.M., Arango, H.G., Broquet, G., Powell, B.S., Weaver, A.T., Zavala-Garay, J., 2011. The regional ocean modeling system (ROMS) 4-dimensional variational data assimilation systems: Part I – system overview and formulation. Prog. Oceanogr. (ISSN: 0079-6611) 91 (1), 34–49. http://dx.doi.org/10.1016/j.pocean.2011.05.004, URL https://www.sciencedirect.com/science/article/pii/S0079661111000516.

Novellino, A., Arnaud, A., Schiller, A., Wan, L., 2024. End user applications for ocean forecasting: present status description. State Planet Discuss http://dx.doi.org/10.5194/sp-2024-25.

Polinov, S., Bookman, R., Levin, N., 2021. Spatial and temporal assessment of oil spills in the mediterranean sea. Marine Poll. Bull. (ISSN: 0025-326X) 167, 112338. http://dx.doi.org/10.1016/j.marpolbul.2021.112338.

Prigent, A., Poulain, P., Besio, M.M.G., 2017. Comparison between Stokes drift and wind induced slip of mediterranean drifters. Rel. OGS 2017/78 OCE 20 MAOS 21, https://hdl.handle.net/20.500.14083/22030.

Rascle, N., Ardhuin, F., 2013. A global wave parameter database for geophysical applications. Part 2: Model validation with improved source term parameterization. Ocean. Model. (ISSN: 1463-5003) 70, 174–188. http://dx.doi.org/10.1016/j.ocemod.2012.12.001, URL https://www.sciencedirect.com/science/article/pii/S1463500312001709. Ocean Surface Waves.

REMPEC, 2019. 2018 corsica oil spill. URL https://www.rempec.org/en/our-work/pollution-preparedness-and-response/response/accident-map/2018-corsica-oil-spill.

Saha, S., Moorthi, S., Pan, H.-L., Wu, X., Wang, J., Nadiga, S., Tripp, P., Kistler, R., Woollen, J., Behringer, D., Liu, H., Stokes, D., Grumbine, R., Gayno, G., Wang, J., Hou, Y.-T., Chuang, H.-Y., Juang, H.-M., Sela, J., Goldberg, M., 2010. The NCEP climate forecast system reanalysis. Bull. Am. Meteorol. Soc. - BULL AMER METEOROL SOC 91, http://dx.doi.org/10.1175/2010BAMS3001.1.

Saha, S., Moorthi, S., Wu, X., Wang, J., Nadiga, S., Tripp, P., Behringer, D., Hou, Y.-T., Chuang, H.-y., Iredell, M., et al., 2014. The NCEP climate forecast system version 2. J. Clim. 27 (6), 2185–2208.

Sayol, J., Orfila, A., Simarro, G., Conti, D., Renault, L., Molcard, A., 2014. A Lagrangian model for tracking surface spills and SaR operations in the ocean. Environ. Model. Softw. (ISSN: 1364-8152) 52, 74–82. http://dx.doi.org/10.1016/j.envsoft.2013.10.013.

Shom, 2017. Modèle hydrodynamique 3D d'évolution de l'océan. https://services.data.shom.fr:/geonetwork/srv/.

Skamarock, W., Klemp, J., Dudhia, J., Gill, D., Barker, D., Wang, W., Powers, J., 2008. A Description of the Advanced Research WRF Version 3, A Description of the Advanced Research WRF Version 3, vol. 27.3–27,

Tolman, H.L., et al., 2014. User Manual and System Documentation of WAVEWATCH III version 5.16. (Technical Note 316), NOAA / NWS / NCEP / MMAB, College Park, MD, USA, Available online at https://polar.ncep.noaa.gov/waves/wavewatch/manual.v5.16.pdf.

Valenciaport, 2024. Freight traffic at valenciaport grows by 10% in 2024. URL https://www.valenciaport.com/en/freight-traffic-at-valenciaport-grows-by-10-in-2024/.

Van Sebille, E., Griffies, S.M., Abernathey, R., Adams, T.P., Berloff, P., Biastoch, A., Blanke, B., Chassignet, E.P., Cheng, Y., Cotter, C.J., Deleersnijder, E., Döös, K., Drake, H.F., Drijfhout, S., Gary, S.F., Heemink, A.W., Kjellsson, J., Koszalka, I.M., Lange, M., Lique, C., MacGilchrist, G.A., Marsh, R., Mayorga Adame, C.G., McAdam, R., Nencioli, F., Paris, C.B., Piggott, M.D., Polton, J.A., Rühs, S., Shah, S.H., Thomas, M.D., Wang, J., Wolfram, P.J., Zanna, L., Zika, J.D., 2018. Lagrangian ocean analysis: Fundamentals and practices. Ocean. Model. (ISSN: 1463-5003) 121, 49–75. http://dx.doi.org/10.1016/j.ocemod.2017.11.008.

Van Sebille, E., Kehl, C., Lange, M., Delandmeter, P., 2023. Parcels. http://dx.doi.org/10.5281/zenodo.8010997, URL https://github.com/OceanParcels/parcels.

Visconti, G., Ruggieri, P., 2020. Non-linearities, randomness and chaos. In: Fluid Dynamics: Fundamentals and Applications. Springer International Publishing, Cham, pp. 205–251. http://dx.doi.org/10.1007/978-3-030-49562-6_7.

Wecel, K., Strozyna, M., Szmydt, M., Abramowicz, W., 2024. The impact of cruises on maritime traffic: A case study of the COVID-19 pandemic and the war in Ukraine. Netw. Spat. Econ. 64–72. http://dx.doi.org/10.1007/s11067-023-09612-0.

Yang, Y., Li, Y., Li, J., Liu, J., Gao, Z., Guo, K., Yu, H., 2021. The influence of Stokes drift on oil spills: Sanchi oil spill case. Acta Ocean. Sin. 40, 30–37. http://dx.doi.org/10.1007/s13131-021-1889-9.